Fermi National Accelerator Laboratory

FERMILAB Pub-94/171-E
CDF

Analysis of Jet Charged Particle Momentum Distributions for Quark-Gluon Separation in $\bar{p}p$ Collisions at $\sqrt{s}$ = 1.8 TeV

The CDF Collaboration

Fermi National Accelerator Laboratory
P.O. Box 500, Batavia, Illinois 60510

June 1994

Submitted to *Physical Review D*

Operated by Universities Research Association Inc. under Contract No. DE-AC02-76CHO3000 with the United States Department of Energy

Disclaimer

CDF/PUB/JET/PUBLIC/2216
FERMILAB-PUB-94/171-E

Analysis of jet charged particle momentum distributions for quark-gluon separation in $\bar{p}p$ collisions at $\sqrt{s}$=1.8 TeV

THE CDF COLLABORATION

F. Abe,[11] M. Albrow,[6] D. Amidei,[14] C. Anway-Wiese,[3] G. Apollinari,[22] M. Atac,[6] P. Auchincloss,[21] P. Azzi,[16] A. R. Baden,[8] N. Bacchetta,[15] W. Badgett,[14] M. W. Bailey,[20] A. Bamberger,[6,a] P. de Barbaro,[21] A. Barbaro-Galtieri,[12] V. E. Barnes,[20] B. A. Barnett,[10] G. Bauer,[13] T. Baumann,[8] F. Bedeschi,[19] S. Behrends,[2] S. Belforte,[19] G. Bellettini,[19] J. Bellinger,[27] D. Benjamin,[26] J. Benlloch,[13] J. Bensinger,[2] A. Beretvas,[6] J. P. Berge,[6] S. Bertolucci,[7] K. Biery,[17,a] S. Bhadra,[9] M. Binkley,[6] D. Bisello,[16] R. Blair,[1] C. Blocker,[2] A. Bodek,[21] V. Bolognesi,[19] A. W. Booth,[6] C. Boswell,[10] G. Brandenburg,[8] D. Brown,[8] E. Buckley-Geer,[6] H. S. Budd,[21] G. Busetto,[16] A. Byon-Wagner,[6] K. L. Byrum,[1] C. Campagnari,[6] M. Campbell,[14] A. Caner,[6] R. Carey,[8] W. Carithers,[12] D. Carlsmith,[27] J. T. Carroll,[6] R. Cashmore,[6,a] A. Castro,[16] F. Cervelli,[19] K. Chadwick,[6] J. Chapman,[14] G. Chiarelli,[7] W. Chinowsky,[12] S. Cihangir,[6] A. G. Clark,[6] M. Cobal,[19] D. Connor,[17] M. Contreras,[4] J. Cooper,[6] M. Cordelli,[7] D. Crane,[6] J. D. Cunningham,[2] C. Day,[6] F. DeJongh,[6] S. Dell'Agnello,[19] M. Dell'Orso,[19] L. Demortier,[22] B. Denby,[6] P. F. Derwent,[14] T. Devlin,[23] D. DiBitonto,[24] M. Dickson,[21] R. B. Drucker,[12] K. Einsweiler,[12] J. E. Elias,[6] R. Ely,[12] S. Eno,[4] S. Errede,[9] A. Etchegoyen,[6,a] B. Farhat,[13] M. Frautschi,[15] G. J. Feldman,[8] B. Flaugher,[6] G. W. Foster,[6] M. Franklin,[8] J. Freeman,[6] H. Frisch,[4] T. Fuess,[6] Y. Fukui,[11] A. F. Garfinkel,[20] A. Gauthier,[9] S. Geer,[6] D. W. Gerdes,[4] P. Giannetti,[19] N. Giokaris,[22] P. Giromini,[7] L. Gladney,[17] M. Gold,[15] J. Gonzalez,[17] K. Goulianos,[22] H. Grassmann,[16] G. M. Grieco,[19] R. Grindley,[17,a] C. Grosso-Pilcher,[4] C. Haber,[12] S. R. Hahn,[6] R. Handler,[27] K. Hara,[25] B. Harral,[17] R. M. Harris,[6] S. A. Hauger,[5] J. Hauser,[3] C. Hawk,[23] T. Hessing,[24] R. Hollebeek,[17] L. Holloway,[9] S. Hong,[14] G. Houk,[17] P. Hu,[18] B. Hubbard,[12] B. T. Huffman,[18] R. Hughes,[21] P. Hurst,[8] J. Huth,[6] J. Hylen,[6] M. Incagli,[19] T. Ino,[25] H. Iso,[25] H. Jensen,[6] C. P. Jessop,[8] R. P. Johnson,[6] U. Joshi,[6] R. W. Kadel,[12] T. Kamon,[24] S. Kanda,[25] D. A. Kardelis,[9] I. Karliner,[9] E. Kearns,[8] L. Keeble,[24] R. Kephart,[6] P. Kesten,[2] R. M. Keup,[9] H. Keutelian,[6] D. Kim,[6] S. B. Kim,[14] S. H. Kim,[25] Y. K. Kim,[12] L. Kirsch,[2] K. Kondo,[25] J. Konigsberg,[8] K. Kordas,[17,a] E. Kovacs,[6] M. Krasberg,[14] S. E. Kuhlmann,[1] E. Kuns,[23] A. T. Laasanen,[20] S. Lammel,[3] J. I. Lamoureux,[27] S. Leone,[19] J. D. Lewis,[6] W. Li,[1] P. Limon,[6] M. Lindgren,[3] T. M. Liss,[9] N. Lockyer,[17] M. Loreti,[16] E. H. Low,[17] D. Lucchesi,[19] C. B. Luchini,[9] P. Lukens,[6] P. Maas,[27] K. Maeshima,[6] M. Mangano,[19] J. P. Marriner,[6] M. Mariotti,[19]

Submitted to Physical Review D June 22, 1994.

R. Markeloff,[27] L. A. Markosky,[27] J. Matthews,[15] R. Mattingly,[2] P. McIntyre,[24] A. Menzione,[19] E. Meschi,[19] T. Meyer,[24] S. Mikamo,[11] M. Miller,[4] T. Mimashi,[25] S. Miscetti,[7] M. Mishina,[11] S. Miyashita,[25] Y. Morita,[25] S. Moulding,[2] J. Mueller,[23] A. Mukherjee,[6] T. Muller,[3] L. F. Nakae,[2] I. Nakano,[25] C. Nelson,[6] D. Neuberger,[3] C. Newman-Holmes,[6] J. S. T. Ng,[8] M. Ninomiya,[25] L. Nodulman,[1] S. Ogawa,[25] R. Paoletti,[19] V. Papadimitriou,[6] A. Para,[6] E. Pare,[8] S. Park,[6] J. Patrick,[6] G. Pauletta,[19] L. Pescara,[16] G. Piacentino,[19] T. J. Phillips,[5] F. Ptohos,[8] R. Plunkett,[6] L. Pondrom,[27] J. Proudfoot,[1] G. Punzi,[19] D. Quarrie,[6] K. Ragan,[17,a] G. Redlinger,[4] J. Rhoades,[27] M. Roach,[26] F. Rimondi,[6,a] L. Ristori,[19] W. J. Robertson,[5] T. Rodrigo,[6] T. Rohaly,[17] A. Roodman,[4] W. K. Sakumoto,[21] A. Sansoni,[7] R. D. Sard,[9] A. Savoy-Navarro,[6] V. Scarpine,[9] G. Sciacca,[19] O. Schneider,[12] M. H. Schub,[20] R. Schwitters,[8] A. Scribano,[19] S. Segler,[6] S. Seidel,[15] Y. Seiya,[25] G. Sganos,[17,a] M. Shapiro,[12] N. M. Shaw,[20] M. Sheaff,[27] M. Shochet,[4] J. Siegrist,[12] A. Sill,[21] P. Sinervo,[17,a] J. Skarha,[10] K. Sliwa,[26] D. A. Smith,[19] F. D. Snider,[10] L. Song,[6] T. Song,[14] M. Spahn,[12] A. Spies,[10] P. Sphicas,[13] R. St. Denis,[8] L. Stanco,[6,a] A. Stefanini,[19] G. Sullivan,[4] K. Sumorok,[13] R. L. Swartz, Jr.,[9] M. Takano,[25] K. Takikawa,[25] S. Tarem,[2] F. Tartarelli,[19] S. Tether,[13] D. Theriot,[6] M. Timko,[26] P. Tipton,[21] S. Tkaczyk,[6] A. Tollestrup,[6] J. Tonnison,[20] W. Trischuk,[8] Y. Tsay,[4] J. Tseng,[10] N. Turini,[19] F. Ukegawa,[25] D. Underwood,[1] S. Vejcik, III,[14] R. Vidal,[6] R. G. Wagner,[1] R. L. Wagner,[6] N. Wainer,[6] R. C. Walker,[21] J. Walsh,[17] G. Watts,[21] T. Watts,[23] R. Webb,[24] C. Wendt,[27] H. Wenzel,[19] W. C. Wester, III,[12] T. Westhusing,[9] S. N. White,[22] A. B. Wicklund,[1] E. Wicklund,[6] H. H. Williams,[17] B. L. Winer,[21] J. Wolinski,[24] D. Y. Wu,[14] X. Wu,[19] J. Wyss,[16] A. Yagil,[6] K. Yasuoka,[25] Y. Ye,[17,a] G. P. Yeh,[6] C. Yi,[17] J. Yoh,[6] M. Yokoyama,[25] J. C. Yun,[6] A. Zanetti,[19] F. Zetti,[19] S. Zhang,[14] W. Zhang,[16] S. Zucchelli,[6,a]

The CDF Collaboration

[1] *Argonne National Laboratory, Argonne, Illinois 60439*

[2] *Brandeis University, Waltham, Massachusetts 02254*

[3] *University of California at Los Angeles, Los Angeles, California 90024*

[4] *University of Chicago, Chicago, Illinois 60637*

[5] *Duke University, Durham, North Carolina 27706*

[6] *Fermi National Accelerator Laboratory, Batavia, Illinois 60510*

[7] *Laboratori Nazionali di Frascati, Istituto Nazionale di Fisica Nucleare, Frascati, Italy*

[8] *Harvard University, Cambridge, Massachusetts 02138*

[9] *University of Illinois, Urbana, Illinois 61801*

[10] *The Johns Hopkins University, Baltimore, Maryland 21218*

[11] *National Laboratory for High Energy Physics (KEK), Japan*

[12] *Lawrence Berkeley Laboratory, Berkeley, California 94720*

[13] *Massachusetts Institute of Technology, Cambridge, Massachusetts 02139*

[14] *University of Michigan, Ann Arbor, Michigan 48109*

[15] *University of New Mexico, Albuquerque, NM 87131*

(16) *Universita di Padova, Instituto Nazionale di Fisica Nucleare, Sezione di Padova, I-35131 Padova, Italy*
(17) *University of Pennsylvania, Philadelphia, Pennsylvania 19104*
(18) *University of Pittsburgh, Pittsburgh, PA 15260*
(19) *Istituto Nazionale di Fisica Nucleare, University and Scuola Normale Superiore of Pisa, I-56100 Pisa, Italy*
(20) *Purdue University, West Lafayette, Indiana 47907*
(21) *University of Rochester, Rochester, New York 15627*
(22) *Rockefeller University, New York, New York 10021*
(23) *Rutgers University, Piscataway, New Jersey 08854*
(24) *Texas A&M University, College Station, Texas 77843*
(25) *University of Tsukuba, Tsukuba, Ibaraki 305, Japan*
(26) *Tufts University, Medford, Massachusetts 02155*
(27) *University of Wisconsin, Madison, Wisconsin 53706*

Abstract

An analysis of charged particle distributions in jets has been performed for dijet and photon+jet events from $\bar{p}p$ collisions at $\sqrt{s}$=1.8 TeV in the Collider Detector at Fermilab(CDF). The resulting distributions are compared with those from the QCD inspired Monte Carlo programs, HERWIG and PYTHIA. The gluon fractions of the CDF jet samples are estimated from charged particle multiplicities, and from a likelihood function obtained with the two Monte Carlo programs. This comparison yields the result that jets in the dijet process are gluon rich, while jets recoiling against photons are quark rich. This result is consistent with the QCD predictions for the sub-process cross sections.

1 Introduction

The difference between quark-initiated and gluon-initiated jets is a subject of long-standing interest [1−9]. There have been some positive reports for these differences [1−4,6], but so far the overall results are not conclusive. Recently, jets with high transverse momenta have been produced copiously at the Tevatron collider at $\sqrt{s}$ =1.8 TeV and observed with the CDF detector. The observed jets have high charge multiplicities, and the statistical significance of quantities which characterize the hadronization of an individual jet are expected to be higher than those obtained in preceding experiments. The higher energies of jets observed at CDF allow a more precise definition of fragmentation quantities and the use of different quark/gluon tagging methods provides a complementary approach to tests at e^+e^- colliders.

To examine the differences between quark and gluon jets, one must obtain quark-enriched and gluon-enriched samples, or know the ratio of gluons to quarks in the samples. Here we review methods which have been used in e^+e^- annihilation and $\bar{p}p$ collider experiments. The hadrons produced in a majority of e^+e^- annihilation events show a clear two-jet structure with a jet angular distribution consistent with the process $e^+e^- \to q\bar{q}$. In addition, a fraction of events show a three jet structure resulting from hard gluon radiation: $e^+e^- \to q\bar{q}g$. Some methods in e^+e^- annihilation are based on these two samples, although details of the analysis are different. In the experiments JADE and TPC [1, 2], the lowest energy jet in the three-jet event is tagged as a gluon jet and the other jets as quark jets. The AMY collaboration[3] defined the gluon jet in a three jet process such that it is opposite to the largest opening angle between the other two jets. The OPAL collaboration[4] used lepton tagging to identify a quark jet among two jets with lower energy in a three jet event. The remaining jet was regarded as a gluon jet. On the other hand, HRS, MARK-II

and TASSO selected three-fold-symmetric three-jet events [5, 6, 7], in which all three jets had nearly equal energies, and compared these to dijet events.

The HRS collaboration[5] compared the charged multiplicities of quark and gluon jets, and reported no differences within experimental errors: $< n >_g / < n >_q = 1.29^{+0.21}_{-0.41} \pm 0.20$. The Mark-II collaboration [6] studied the inclusive momentum spectrum of particles and reported a softer fragmentation in gluon jets. In a similar study, the TASSO collaboration[7], however, obtained a negative result, and pointed out that the Mark-II used different cuts on charged multiplicities for the 2 jet and the 3 jet events which possibly gave rise to the observed difference. The JADE collaboration[1] observed that gluon jets tend to carry a higher average transverse momentum than quark jets; $< p_T >_3 / < p_T >_2 = 1.16 \pm 0.02$. Recently the AMY collaboration reported that the rapidity of the leading (i.e. highest E_T) particle, the core energy fraction and the integrated energy-energy correlation indicates a softer fragmentation of gluons[3].

In hadron colliders, the UA1 collaboration[8] exploited the difference in the kinematical ranges occupied by quarks and gluons to perform a statistical separation of quark and gluon jets, and obtained a quark-enriched and a gluon-enriched sample of dijet events. Using these samples, they showed that quark jets have, on average, a harder fragmentation spectrum and a higher degree of collimation. They also gave a result on the average charge of jets, showing that gluon-enriched jets are neutral, whereas quark-enriched jets show a significant non-zero average charge. This UA1 method cannot be used with CDF because gluon jets dominate in this energy scale ($E_T < 100$ GeV).

Although QCD describes the jet production cross sections and jet axis angular distributions, the non-perturbative phase of jet development is very complex and the

predictive power of QCD is still quite limited.

Among the presently used phenomenological models for hadronization, the cluster [10, 11, 12] and string [13] models with parton-shower scheme incorporate the concept of planar color flow. The differences in the color flow in the quark and gluon jets generate differences in their fragmentation distributions. In this analysis we use two Monte Carlo programs, PYTHIA version 5.6 [15, 16] and HERWIG version 5.6[14], which are based on the string and cluster models, respectively.

For the study of the jet internal variables in this article, we use two sets of data which are expected from perturbative QCD to contain different fractions of quark and gluon jets. They are a) jets in the dijet process and b) jets associated with direct photons. The elementary processes involved in the dijet process are typical QCD $2 \rightarrow 2$ processes. The lowest order Feynman graphs for the process are shown in Fig. 1(a). In the energy region we are dealing with in this paper, gluon jets are expected to dominate the final state. The Feynman graphs for the direct photon processes are shown in Fig. 1(b). The Compton effect($gq \rightarrow \gamma q$) gives the largest contribution to the direct photon process, hence the jets associated with direct photons are expected to be quark jet enriched. However, the experimental separation of a single photon from overlapping photons from $\pi^0 \rightarrow \gamma\gamma$ or $\eta \rightarrow \gamma\gamma$ or $K_s^0 \rightarrow \pi^0\pi^0$ decays can only be made statistically. Hence, the photon + jet data set generally includes a QCD background in which one gluon hadronizes into a hard neutral meson, π^0 or η or K_s^0. Jets from this process are expected to be more gluon rich than those from the direct photon process and therefore contribute an additional gluon jet background to the experimental signature.

In Section 2, we describe how we selected events for the processes discussed above. Monte Carlo generation of simulated events is discussed in Section 3. The selection

criteria of charged particles associated with jets are given in Section 4. Among other variables, the charged particle multiplicity of a jet is shown from the simulation to have a high separation power between quark and gluon jets. Section 5 is devoted to a comparison of observed multiplicities with those from the simulation for various processes. In Section 6, we describe a moment analysis of the jet fragmentation variables and discuss moment distributions in observed jets. To evaluate the gluon fraction in a given data set, we adopt the quark/gluon likelihood function obtained from the moment analysis. Application of the method to CDF data and comparison of results with quark/gluon fractions predicted from QCD cross sections for subprocesses are presented in Section 7. Separation of quark and gluon jets with multiplicity only and with different combinations of the jet fragmentation variables will also be discussed in this section. Section 8 is a summary of the results.

2 Experimental Data Sets

The CDF detector used during the 1988-89 run has been described in detail in ref. [17]. Taking the center of the detector as the origin, we define the Z-axis along the proton beam direction, X- and Y-axes as horizontal and vertical(up) directions, respectively. The polar and azimuthal angles are denoted by θ and ϕ, respectively, and pseudo-rapidity, η, is defined as: $\eta = -\ln[\tan(\theta/2)]$. In this analysis, only jets reconstructed in the central calorimeters are used. There are two tracking chambers, the vertex time projection chambers and the central tracking chamber (CTC). The CTC fully covers $|\eta| < 1.0$, and has a transverse momentum resolution of $\Delta p_T/p_T^2 = 0.0011\ (\mathrm{GeV}/c)^{-1}$. Track-finding efficiency in the jet core (i.e. for particles with rapidity w.r.t the jet axis greater than 2) was measured to be greater than 85% with an uncertainty of 7% [18]. Outside of the CTC are the central electromagnetic (CEM),

central hadronic and endwall hadronic calorimeters. These are arranged in projective towers of size $\Delta\eta = 0.1$ by $\Delta\phi = 0.26$. Proportional wire chambers with cathode strips perpendicular to the wires, termed the central strip chambers (CES), are embedded in the CEM at a depth of six radiation lengths, where the electromagnetic shower reaches its maximum.

For this analysis, we selected data sets for the dijet and photon + jet processes obtained by CDF in $\bar{p}p$ collisions at $\sqrt{s}$ =1.8 TeV with an integrated luminosity of 4.2 pb^{-1} and 3.3 pb^{-1}, respectively.

Dijet events at CDF are selected according to hardware trigger conditions[19]. We have chosen two data subsets with E_T thresholds of 20 GeV and 40 GeV, which were collected by triggers prescaled to accept 1 in 300 and 1 in 30 events, respectively. From perturbative QCD, one expects these samples to be gluon jet enriched. Jets are defined as energy clusters in the calorimeters found by using a fixed-cone algorithm [20] with a radius $R = \sqrt{\Delta\eta^2 + \Delta\phi^2}$ of 0.7. The momentum of a jet is defined by the sum of momentum vectors pointing to the center of the calorimeter towers within the cone. Thus the invariant mass of the jet is well defined in the clustering algorithm. To avoid bias from jets near the trigger threshold, events are excluded if the leading jet had an E_T below thresholds of 30 GeV and 50 GeV, respectively. We require the energy centroid of the leading and the next to leading jets to be in the central region, $0.1 \leq |\eta| \leq 0.7$, and to be within 25° of back-to-back in ϕ to enhance the dijet topology. It was also required that the event vertex, Z_v satisfy the condition $|Z_v| <$ 60 cm.

The second data set is a sample of photon +jet events[21]. Events are selected by requiring an isolated electromagnetic (EM) cluster and one jet opposite in ϕ ($\Delta\phi =$ 180° $\pm$ 25°) in the central region. An E_T balance between the EM cluster and the

jet is required by the condition, $0.6 < E_T^{em}/E_T^j < 1.67$. The photon identification requires the sharing of the lateral shower energy between CEM towers to be consistent with that for a photon or electron induced shower. Strip and wire clusters in CES are required to have approximately equal energies, and their cluster centroids should be well within the active region of the CES chamber. In addition, the ratio of hadron-to-EM cluster energy is required to be less than 0.05. Finally we require no tracks pointing at the towers in the cluster.

The photon+jet events selected using the above criteria are expected to consist of both direct photon and π^0(or η or K_s^0)+jet events. To differentiate a single photon from multiple photons from neutral mesons, we employ a χ^2 test for the lateral EM shower distributions at shower maximum as measured by wire and strip projections from the CES chambers [21, 22]. Reference distributions are provided from a study of shower development using electrons as well as reconstructed $\rho^{\pm} \to \pi^{\pm}\pi^0$ and $\eta \to \gamma\gamma$ events. An example of χ^2 distributions for the γ+jet events is shown in Fig. 2 in comparison with π^0+jet events obtained with ISAJET[23] and a Monte Carlo shower simulation. We generate two data sets, one with $\chi^2 < 4$ labeled as "γ"+jet , and the other with $5 < \chi^2 < 20$ termed as "π^0"+jet . A data set with $\chi^2 < 20$ is labeled as "γ/π^0"+jet . An isolation requirement $I = \left(E_T(R = 0.7) - E_T^{EM}\right)/E_T^{EM} \leq 0.15$ is also made for the "γ"+jet sample. Here, E_T^{EM} and $E_T(R = 0.7)$ are the transverse energy of the EM cluster and the total transverse energy within a cone of radius $R = 0.7$ centered on the EM cluster, respectively. On the other hand, γ+jet (π^0+jet) without " " represents a pure data set of γ (π^0) + jet events. From Fig. 2, the "γ"+jet data set is estimated to include approximately 65% of γ+jet events, while the γ+jet event fraction in the "π^0"+jet data set is about 35%. The γ fraction in the "γ"+jet sample or in the "π^0"+jet sample, F_γ, is determined according to the method described in

ref. [21] for $\chi^2 < 4$ or $5 < \chi^2 < 20$, respectively, in each E_T bin.

The total number of jets in each of the data sets are listed in Table 1 as a function of jet E_T. Trigger thresholds and different scale factors of data samples screen off the exponential decrease of the number of jets with E_T.

3 Monte Carlo Data Sets

Monte Carlo data samples for gluon and quark jets in the dijet channel were generated as follows. We first produced quark and gluon jets in QCD $2 \rightarrow 2$ processes at $\sqrt{s}$ =1.8 TeV by using the event generators PYTHIA and HERWIG. We selected events with final states involving purely quarks(antiquarks) or gluons (i.e. no $qg \rightarrow qg$). The generated events were then processed through a detector simulation program which realistically reproduces the CDF detectors including track-finding inefficiency. The events were then reconstructed with the same fixed-cone clustering algorithm and the same dijet selection cuts used for the real data. Finally, the events were divided into eight samples, according to jet E_T, with 10 GeV bins spanning 10 to 90 GeV. In each E_T bin, approximately 6000 quark and 6000 gluon jets are retained. The number of jets in each 2 GeV bin was set to 1200 for each quark or gluon jets data so that the E_T distribution is flat in each sample, which is close to the distribution of analyzed CDF data except for the lowest E_T samples. We applied an additional cut of $E_T \geq 14$ GeV to the samples in order to avoid inconsistency in the E_T distributions between Monte Carlo data and the CDF data, which is obvious at $E_T \leq 14$ GeV. Hence, the lowest E_T samples (E_T = 14–20 GeV) have 2000 jets in each 2 GeV bin. We shall call these gluon and quark sets "reference" sets.

In the preceeding section, we indicated that the "γ/π^0"+jet data include neutral mesons+jet events. These events are considered to originate from the QCD

dijet process where an outgoing parton fragments into a leading neutral meson with a large momentum fraction $z = (E(had) + P_Z(had)) / (|E(par) + P_Z(par))$, where $E(had)(P_Z(had))$ and $E(par)(P_Z(par))$ are the energy (the longitudinal momentum) of the hadron(i.e. π^0) and the parent parton generated in the hard collisions. To simulate such events, we generated a large number of QCD dijet events with HERWIG and created a set of events by applying, after a full detector simulation, the same cut conditions as to the "γ/π^0"+jet sample in the real data. By comparing the simulated EM clusters with mesons at the generator level, it was found that the π^0, η and K_s^0 mesons with a momentum fraction $z > 0.7$ are dominant in this sample.

4 Charged Particles Associated with Jets

First, tracks with transverse momentum less than 0.4 GeV/c in the lab system were excluded as these low momentum tracks are curled and not reconstructed in the magnetic field of 1.41 T. Tracks associated with a jet were selected by requiring that the impact parameter relative to the event vertex should be less than 0.5 cm and the z position of the track at the point of closest approach to the Z-axis should be within 60 cm of the center of the detector. Tracks inside a cone were selected if they had a minimum pseudorapidity with respect to the jet axis, $\eta_T(track) \geq 1.2$, where $\eta_T(track)$ is defined as $\eta_T(track) \equiv \frac{1}{2}\left[|P(track)| + P_L(track)\right] / \left[|P(track)| - P_L(track)\right]$. $P(track)$ and $P_L(track)$ are the track momentum and the longitudinal momentum along the jet axis in the lab system, respectively. An additional cut of $|P_L(track)| \geq 0.3$ GeV/c was also applied to find tracks associate with the jet.

Throughout this analysis, we treat jets in their rest frames which are defined by their 4-momenta as measured by the calorimeters. In the transformation of the momenta of charged particles from the laboratory to the jet rest frame, masses of all

charged particles are assumed to be equal to the pion mass.

Because moments of the charged particle momentum are calculated in the jet rest frame, an ambiguity is introduced for the proper definition of the jet momenta since in the lab system there are soft particles which may belong either to the jet or to the underlying event. The soft particles do not give substantial effects in the determination of the jet c.m. frame, but they acquire large backward momenta by the Lorentz boost to the jet c.m. frame, giving non-trivial contributions to the jet momenta. To avoid this effect, we sum only over particles whose momenta lie in the angular range less than 135° from the forward jet axis in the jet c.m. momentum space. In a simulation study using the PYTHIA generator, this cut eliminates approximately 60 % of particles from underlying events while keeping 90% of particles from hard collisions at $E_T = 30 - 40$ GeV.

5 Charged Multiplicity in a Jet

An observable that may carry information to identify a parton species is the particle multiplicity in a jet. The average multiplicity in a gluon jet is expected to be higher than that in a quark jet [24, 25, 26, 27]. In the asymptotic limit, i.e. $Q^2 \to \infty$, the ratio of multiplicities for quark and gluon jets is expected to be

$$\frac{\langle n \rangle_g}{\langle n \rangle_q} = \frac{C_A}{C_F} = \frac{9}{4}\,, \tag{1}$$

where C_F and C_A are the color factor and the number of colors (i.e., $C_F = 4/3$, $C_A = 3$ for QCD), respectively. The values of Q^2 experimentally accessible are far from asymptotic [12], hence agreement of Eq.(1) with experimental results is rather poor [1–8]. Higher order calculations [28] result in smaller differences between quark

and gluon jets than Eq.(1) predicts :

$$\frac{\langle n\rangle_g}{\langle n\rangle_q} = \frac{9}{4}\left\{1 - \left(1 + \frac{N_f}{C_A} - \frac{2N_fC_F}{C_A^2}\right)\left[\sqrt{\frac{\alpha_s C_A}{18\pi}} + \frac{\alpha_s C_A}{18\pi}\left(\frac{25}{8} - \frac{3}{4}\frac{N_f}{C_A} - \frac{N_fC_F}{C_A^2}\right)\right]\right\}, \tag{2}$$

where N_f is the number of flavors. On the other hand, an empirical equation was proposed by Webber in ref.[12], in which the correction magnitude is of order $\sqrt{\alpha_s}$ which is proportinal to $\{\ln(E(jet)/\Lambda_{QCD})\}^{-\frac{1}{2}}$.

Figures 3(a) $\sim$ (f) show the distribution of charged multiplicity for both the Monte Carlo and CDF data. Entries with charged multiplicity less than 2 are excluded. In Figs. 3(a)$\sim$(d), histograms with solid lines correspond to the Monte Carlo quark jet and those with dot-dashed lines to the Monte Carlo gluon jet. One observes that Monte Carlo quark jets have lower multiplicities than Monte Carlo gluon jets as was expected from the higher color charge of the gluon and the above predictions. The open circles in Figs. 3(a)$\sim$(b) show the multiplicities in the CDF dijet data. These closely resemble the distributions from the Monte Carlo gluon jets. The open circles in Figs. 3(c)$\sim$(d) show the multiplicity distribution for the CDF "γ"+jet events. The distributions are more quark-like than those for the dijet events. For completeness in Figs. 3(e)$\sim$(f), we compare CDF dijet and "γ"+jet data directly.

The charged multiplicities in the PYTHIA and CDF jets with multiplicities more than 1 are listed in Table 2 for the two processes in various E_T ranges. The mean values of the charged multiplicity in CDF dijet data are larger than those in CDF "γ"+jet data over all E_T regions. This relative difference is close to that predicted between Monte Carlo gluon jets and quark jets. However, the CDF data lie systematically higher than the Monte Carlo predictions for either hard scattering process. This difference is sensitive to the tracking efficiency and within the systematic uncertainty associated with this of 7 %, is not significant at $E_T > 30$ GeV.

6 Moment Analysis of Fragmentation

The charged multiplicity in a jet shows a clear statistical difference between quarks and gluons [1−8]. In the following analysis, however, we do not try to find *ad hoc* variables which are more sensitive than others for differences between the parton ancestors. Instead, we adopt a systematic approach of analyzing the momentum distribution (the fragmentation function) of charged particles in a jet by using the method of moment analysis [29, 30]. This is motivated by the fact that a function (i.e. the momentum distribution function) of variables (i.e. the momenta of charged particles) can generally be expressed as a linear combination of its moments as defined by the Mellin transform. More terms of successively higher orders will reproduce the function more precisely.

The variables chosen can be divided into two classes which we call the "mechanical moments" and the "electric moments". The mechanical moments are the m-th power of the momentum, summed over all particles: $\sum_{i=1}^{n}(k_{Li}/M)^m$ and $\sum_{i=1}^{n}(k_{Ti}/M)^m$, where the term $(k_i/M)^m$ represents the m-th power of the normalized momentum of the i-th charged particle, n is the total number of charged particles in a jet, and M is the invariant mass of the jet. The subscript L and T indicate the longitudinal and transverse momentum components to the jet axis, respectively. The other class, the electric moments, are the m-th power of the momentum multiplied by the electric charge of the particle and summed over all particles: $\sum_{i=1}^{n} Q_i(k_{Li}/M)^m$ and $\sum_{i=1}^{n} Q_i(k_{Ti}/M)^m$, where Q_i is the charge of the i-th particle.

A set of 10 variables was chosen as follows : The moment variables of each track have four degrees of freedom, i.e. three degrees of freedom of the moments and one for the charge of a particle. The moment variables have another degree of freedom of the jet invariant mass M. Since we exclude jets with fewer than two charged

particles, the minimum number of degrees of freedom of the jet system is $2 \times 4 + 1 = 9$. Eight moment variables were determined by considering the number of degrees of freedom and the symmetrical selection of moments in k_L and k_T, in "mechanical" and "electric" and in the degree of power($m = \pm 2$), which cancels out the individual discrepancy in each moment between the CDF data and the Monte Carlo data as seen in Section 7. The 0-th power of the mechanical moment is applied as the 9-th moment variable, which corresponds to the multiplicity of charged particles. In addition to these moments, we use another measure to distinguish quark and gluon jets ; the ratio of the electromagnetic calorimeter energy to the total calorimeter energy of a jet (EM fraction). The gluon jets and the CDF dijets have higher EM fractions than the quark jets; this is consistent with the fact that lower momentum particles deposit a higher average fractional energy in the EM calorimeter. These 10 variables are shown in Table 3.

Figures 4(a) $\sim$ (d) show logarithmic distributions of electric moments for the Monte Carlo and CDF jets in the E_T range of 30 to 40 GeV. They are calculated from the transverse/longitudinal components of particle momenta. All distributions are normalized to unity.

First, we discuss results for the Monte Carlo jets. As an example of moment distributions, we present the moment $Q(k_T/M)^{-2}$ for Monte Carlo quark and gluon jets in Fig. 4(a). In this figure, gluon distributions shown by dashed lines peak at a larger value of the moment than the quark distributions shown by solid lines. On the other hand, distributions of $Q(k_T/M)^2$ show opposite trends for Monte Carlo quark and gluon jets as shown in Fig. 4(b). This can be interpreted as gluon jets being "broader" than quark jets. The longitudinal moments $Q(k_L/M)^{-2}$ and $Q(k_L/M)^2$ are shown in Figs. 4(c) and (d), respectively. In these figures, the quark jets have

larger values of the positive power moments, and lower values of the negative power moments than gluon jets. This means that quark initiated jets are "harder" than gluon jets. The difference between quark jets and gluon jets is clearer in the negative power moments than in the positive ones.

The moment distributions for CDF dijet data are also plotted for the electric moments in Fig. 4 (a)~(d), respectively. In addition, the distributions of EM fraction are shown in Figs. 5 and the moment distributions in the higher E_T range of 40 to 50 GeV are shown in Figs. 6(a) ~ (d). In these figures, we observe that the negative (positive) power moment distributions for the CDF dijets are generally closer to those for Monte Carlo gluon (quark) jets than those expected from the QCD sub-process cross sections. This shows the disagreement in each moment distribution between CDF dijets and Monte Carlo jets. Since negative (positive) power moment distributions emphasize the differences of soft (hard) components in momentum spectra of k_T and k_L, this shows that the CDF dijets have longer tails than Monte Carlo generators in these moment distributions. This discrepancy between the CDF data and Monte Carlo jets is also discussed at the end of the next section.

7 Gluon Fraction in Jet Samples

Gluon Fractions Evaluated from Sub-process Cross Sections Theoretical predictions for gluon fractions of jet samples can be estimated by evaluating the sub-process cross sections given by QCD. In the present analysis, we evaluate the theoretical gluon fraction by using the PYTHIA Monte Carlo program. For each specified process, the same kinematical cuts as applied to jets in the preceding sections were applied to quarks and gluons at the parton level. Results for the dijet and γ(direct photon)+jet processes are shown in Fig. 7. In the γ+jet channel, the production cross section of

quark jets at low E_T is expected to be about an order of magnitude larger than that of gluon jets, based on leading-order QCD. Inclusion of the photon bremsstrahlung process makes this prediction more uncertain. This process is not well understood and no attempt has been made to model it. When going to higher values of E_T (e.g. 80 GeV), the gluon fraction in the dijet events decreases from 80% to 70%, whereas in γ+jet events, it increases from 10% to 20%.

To test our method, we also need to estimate the gluon fraction for π^0+jet events expected from the sub-process cross section. The Monte Carlo events generated as described in Section 3 show that the gluon fraction for π^0+jet events in the measured kinematical region is less than that for typical dijets by $5 - 10\%$.

We estimate the gluon fraction of the "γ"+jet and "π^0"+jet samples by evaluating sub-process cross sections, as follows. We denote the predicted gluon fraction for γ+jet events by $F_g(\gamma + jet)$, that for π^0+jet events by $F_g(\pi^0 + jet)$ and the single γ fraction in the photon candidates by $F_\gamma(\chi^2 < 4)$ as defined in Section 2. The gluon fraction in the mixed sample of "γ"+jet events is then given by

$$F_g(\text{“}\gamma\text{”} + jet) = F_g(\gamma + jet) \cdot F_\gamma + F_g(\pi^0 + jet) \cdot (1 - F_\gamma) \,. \qquad (3)$$

The gluon fraction in the "π^0"+jet events $F_g(\text{“}\pi^0\text{”} + jet)$ is obtained by substituting $F_\gamma(5 < \chi^2 < 20)$ for $F_\gamma(\chi^2 < 4)$ in Eq.(3).

The resulting gluon fractions $F_g(\text{“}\gamma\text{”} + jet)$ and $F_g(\text{“}\pi^0\text{”} + jet)$ are shown in Fig. 8 as a function of jet E_T. The values are evaluated only in the E_T region below 40 GeV because at higher E_T the experimental separation between single photons and π^0's is difficult and F_γ is unknown.

Gluon Fractions by Moments/Likelihood Method The analysis in Section 6 showed that the moment distributions for CDF dijets are consistent with the expectation that gluon jets dominate in the kinematical range of interest. We now use the distri-

butions obtained from the fragmentation models PYTHIA and HERWIG to obtain estimates of the relative fraction of quarks and gluons in our data sample. For a given set of moments $(x_1, ..., x_n)$ a log-likelihood for quark vs. gluon is defined as

$$L(x_1, ..., x_n) \equiv \ln \left[\frac{P_q(x_1, ..., x_n)}{P_g(x_1, ..., x_n)} \right] , \tag{4}$$

where $P_q(x_1, ..., x_n)$ and $P_g(x_1, ..., x_n)$ are normalized distribution functions of variables $(x_1, ..., x_n)$ for the quark and gluon sets, respectively.

The rigorous treatment of the likelihood defined by Eq.(4) requires enormous computer resources, since the correlations between all the variables must be used. In the present treatment, we make the following approximations: a log-likelihood $L_i(x_i)$ given by a single moment x_i is defined by

$$L_i(x_i) \equiv \ln \left[\frac{P_q^{(i)}(x_i)}{P_g^{(i)}(x_i)} \right] , \tag{5}$$

where $P_q^{(i)}(x_i)$ and $P_g^{(i)}(x_i)$ are normalized distribution functions of x_i for the quark and gluon Monte Carlo data sets. A separation power of the individual variables can be defined as

$$s_i \equiv \frac{\Delta_i}{\sigma_i} , \tag{6}$$

where Δ_i is the difference of the mean likelihood for the quark and gluon sets, and σ_i is the combined standard deviation for the two reference distributions ($\sigma_i = \sqrt{(\sigma_g{}^2 + \sigma_q{}^2)/2}$). If the moments x_i are mutually independent, we can define the global likelihood as the sum of the L_i's, while distributions of moments are actually correlated. For simplicity of the treatment, we take an equal-weighted sum,

$$L' = \sum_{i=1}^{n} L_i \tag{7}$$

as an effective likelihood parameter, which we call as the separation function.

The histogram of each moment is divided into 50 bins. A statistical error due to the limited number of Monte Carlo events is assigned to each bin, assuming Gaussian statistics. It should be noted that this kind of statistical error can be reduced by increasing the size of the Monte Carlo reference sample. As above, the error propagation for L' is treated without correlation terms between different variables. Finally, we smooth the L' distribution for the reference samples by assuming that L' is distributed as a Gaussian with the standard deviation $\sigma_{L'}$ which is the square-root of the quadratic sum of the statistical errors as discussed above.

The separation powers of the individual moments are given by s_i of Eq.(6). The separation power for 10 variables at the E_T range of 30−40 GeV are listed in Table 4 for PYTHIA and HERWIG programs, respectively. We note that the multiplicity, the moment $\sum(k_{Ti}/M)^{-2}$ and the longitudinal moments have large separation powers and that, in general, negative power moments are more effective for quark/gluon separation than positive power moments. Also, PYTHIA predicts relatively larger separation powers than HERWIG except for the 10th variable.

The resulting separation function shows different distributions $Q(L')$ for quarks and $G(L')$ for gluons as presented in Figs. 9. The separation power obtained from the separation function is 0.85(PYTHIA) or 0.70(HERWIG) at E_T = 30−40 GeV, showing an improvement over that of multiplicity, 0.79(PYTHIA) or 0.63(HERWIG) , in the same E_T range. In these figures, the separation function distributions for the CDF dijet and "γ"+jet events are also shown.

When given a data set to analyze, we determine a quark vs. gluon likelihood for each jet in the sample. We evaluate the overall fraction of the gluon (or quark) jets included in a particular data sample as follows. The likelihood distribution for the

data set is fitted to a superposition of those for the two reference samples,

$$F_j = X_g G_j + (1 - X_g) Q_j. \tag{8}$$

We find the coefficient, X_g, which minimizes the chi-squared defined by

$$\chi^2 = \sum_{j=1}^{50} \left[\frac{D_j - (X_g G_j + (1 - X_g) Q_j)}{\sigma_j} \right]^2 . \tag{9}$$

In Eqs. (8) and (9), G_j, Q_j and D_j are probabilities for gluon, quark and analysis samples to take the j-th bin of the likelihood histograms, respectively. The dominant uncertainty for χ^2 comes from the statistical error for D_j, hence $\sigma_j \cong \sqrt{D_j/N}$, where N is the number of jets in the analysis sample.

We performed a Monte Carlo study to test the method of determination of gluon fractions by this moment/likelihood analysis. A total of 6000 jets for each of gluon and quark samples in the QCD dijet process were generated by HERWIG for every E_T bin of the analysis. Subsets of 1000 jets in each E_T range were extracted from both gluon and quark samples and samples of 1000 jets with known gluon fractions of 0%, 25%,50%, 75% and 100% were obtained. These samples were then analyzed using the remaining gluon and quark jets (5000 jets in each E_T bin) as the reference samples.

Figure 10 shows χ^2 versus the fitting parameter X_g in Eq. 8 for E_T = 30–40 GeV. Curves correspond to the gluon fractions of the analyzed samples of 0%, 25%, 50%, 75% and 100%, respectively, from left to right. Errors in X_g are determined by the condition $\chi^2 = \chi^2_{min} + 1$. The results are consistent with the input values within 3.3 % at E_T = 30–40 GeV. When the selection of referenced and analyzed jets is changed, the values of X_g at χ^2_{min} fluctuate around the input values by about the order of the evaluated errors. This result is consistent with the evaluated errors due to the statistics of the sample.

The gluon fractions of the Monte Carlo samples obtained by the method vs. the known input values are plotted in Fig. 11 for $20 < E_T < 30$ GeV, $30 < E_T < 40$ GeV, $40 < E_T < 50$ GeV and $50 < E_T < 60$ GeV. The result indicates a consistency of the method. The corresponding analysis of the identical Monte Carlo data samples in which the gluon fraction is determined by a χ^2 fit to the particle multiplicity distribution, is shown in Fig. 12. The results are consistent with those obtained from the full likelihood analysis but with larger errors.

Systematic uncertainties in the gluon fraction Systematic uncertainties in the gluon fraction are estimated as follows.

There is an uncertainty related to the energy correction of a jet. The CDF standard energy correction parameters[31] have been determined by Monte Carlo studies of the QCD dijet process in which gluon jets dominate. With Monte Carlo PYTHIA samples of quark and gluon jets, it was found that the energies of quark jets are over-corrected by $\Delta E_T = 1.2 \sim 1.9$ GeV over the E_T range of 10 to 90 GeV than those of gluon jets. If one uses the same correction parameters for quark and gluon jets in this E_T region, the gluon fraction obtained from the likelihood analysis is lower than the input fraction by $3.4 \sim 4.7$ % in each E_T bin as listed in Table 5 and we take this effect as a systematic uncertainty[32]. There is also an uncertainty in the jet E_T due to the difference between E_T spectra of real data and that assumed for the energy correction. This produces a systematic uncertainty in the gluon fraction of $3.0 \sim 3.7$ % in the E_T range of 10 to 90 GeV.

Another uncertainty results from different Monte Carlo generators. In the dijet process, the gluon fraction found by using HERWIG is higher by 2.1 % to 10.8 % than that found by PYTHIA in the E_T range of 10 to 90 GeV. This value is consistent with the difference of the gluon fraction which was obtained by using jets generated

by HERWIG as references and jets generated by PYTHIA as analyzed samples.

Uncertainty due to the track finding efficiency was estimated by comparison of the gluon fractions obtained by using different Monte Carlo references generated by changing the track finding efficiency in the detector simulation within the uncertainty of 7%. This is also discussed in the later section. In the dijet process, the uncertainty is less than 7 % at $E_T \leq 50$ GeV, while an increase in the tracking efficiency of 7% decreases the gluon fraction by 15 % at $E_T = 80$ to 90 GeV. A decrease in the gluon fraction is also observed in the "π^0"+jet and "γ"+jet samples if the tracking efficiency is increased by 7 % , though the effect becomes unclear at $E_T = 30$ to 50 GeV in the "γ"+jet sample.

The total uncertainty which was obtained from a quadratic sum of the above systematic uncertainties and the statistical uncertainty discussed in the preceeding sub-section is also listed in Table 5. The different contribution of the uncertainties found by different Monte Carlo generators and that in the sign to the value of gluon fraction is considered here. It has the largest uncertainty of 16 % at $E_T = 10$ to 20 GeV and at $E_T = 80$ to 90 GeV and the minimum is found at $E_T = 20$ to 30 GeV.

The theoretical uncertainty due to different structure functions of MRS D_0' and D'_- slightly increases with E_T for the dijet process as shown in Fig. 7. The difference as a function of E_T is listed in Table 5. The maximum is 1.8 % at $E_T = 80$ to 90 GeV. It is less than 1.5 % for the γ+jet process in the E_T range of $10 - 50$ GeV.

Results and Comparison with Values Obtained from Sub-process Cross Sections

To compare the gluon fractions obtained from this moment analysis with those evaluated from the sub-process cross sections, the difference in acceptances of the detector for gluon and quark jets must be taken into account. The difference in efficiencies for the identification of events with gluon jets versus quark jets in the

final state was also corrected. The efficiencies were evaluated for each E_T bin by using the Monte Carlo samples generated by PYTHIA and HERWIG for each process, in which identification of jets with quarks and gluons was unambiguously made. The acceptances for the dijet process are listed in in Table 6. These efficiencies were used to correct gluon fractions determined by the moment analysis.

The fraction of final state gluons in the data sets are plotted in Figs. 13 and 14 as a function of jet transverse energy. The error bars on the gluon fraction are given by a set of $X_g^{(-)}$ and $X_g^{(+)}$ such that $\chi^2(X_g^{(-)}) = \chi^2(X_g^{(+)}) = \chi^2_{min} + 1$, which shows the statistical uncertainty. The dot-dashed lines are the total uncertainty obtained from a quadratic sum of the systematic and statistical uncertainties. Figure 13 shows that dijet samples yield a gluon fraction of 70 % to 80 % in the E_T range of 30 $-$ 90 GeV by PYTHIA, consistent with the values evaluated from the sub-process cross sections (Fig. 7). The gluon fraction at $E_T \leq 50$ GeV by HERWIG is higher by 10 $-$ 15 % than those.

The "γ"+jet samples contain a gluon fraction of 40 % to 60 % at E_T = 20 to 50 GeV as shown in Fig. 14. The gluon fraction of the "π^0"+jet data is higher than that of "γ"+jet by about 10 % to 30 %. Both values are slightly higher than those obtained from the cross sections in the γ+jet and π^0+jet processes and the expected γ/π^0 ratio in the photon candidates (See Fig. 8). However, the difference in the gluon fraction between γ+jet and π^0+jet processes is clearly observed at E_T = 30 to 50 GeV and consistent with the expectation. A summary plot of the gluon fraction versus E_T in dijet and photon+jet processes is plotted in Fig. 15 with the predicted values found by the Monte Carlo study of PYTHIA. Here, the errors are the total uncertainty obtained from a quadratic sum of the systematic and statistical uncertainties.

Evaluation of the Gluon Fraction from the Multiplicity As shown in Table 4,

the multiplicity has the largest separation power among the 10 variables. The gluon fraction can be evaluated by replacing in Eq.(9) the separation functions G_j, Q_j and D_j with multiplicity distributions of the corresponding samples. In Figure 16(a) and (c), the gluon fraction was obtained with the track finding efficiency of about 85 % from 10 moment variables and from the charged multiplicity distributions, respectively. The CDF dijet events have the largest gluon fraction and the "γ"+jet events have the lowest value again among the three samples at E_T=30−50 GeV. However, the gluon fractions are rather higher than those obtained with 10 variables for all three samples. Here, the errors are the statistic uncertainty only obtained by a condition of $\chi^2 = \chi^2_{min} + 1$.

The charged multiplicity distribution is more affected by a change in the track finding efficiency. As the uncertainty in the CDF track finding efficiency is 7%, we obtained the gluon fraction by the charged multiplicity distribution with increasing the tracking efficiency by 7%. Results are shown in Fig. 16(b) and (d). The gluon fractions obtained from the charged multiplicity become lower than the QCD predicted values at E_T = 30 to 80 GeV, while the gluon fraction obtained from 10 variables are not as much affected by this change. The difference between Figs. 16(c) and (d) shows a large uncertainty due to the track finding efficiency when using only the charged multiplicity for the analysis.

Evaluation of the Gluon Fraction from Asymmetric Combination of Variables

Except for EM fraction and the charged multiplicty, we applied a symmetric combination of 8 moment variables in the degree of power ($m = \pm 2$), in k_L and k_T and in the "mechanical" and the "electric" moments for the moment analysis. If the Monte Carlo generators realize the distribution of each moment variable correctly, we can evaluate the gluon fraction using any combination of the variables. Six sets

of asymmetrical combinations of 4 variables are substituted for 10 variables in the moment analysis, i.e. (a) the degree of power is all $m = -2$, (b) all $m = +2$, (c) the transverse moments, (d) the longitudinal moments, (e) the mechanical moments and (f) the electric moments only. A Monte Carlo study shows that the predictability of the gluon fraction for above combinations is within errors of 15 % at $E_T \geq 10$ GeV.

The resulting gluon fractions in the CDF dijet events are shown in Figure 17 for $E_T = 10$ to 90 GeV. Though the gluon fractions show gluon-rich behavior and the decrease with E_T in four combinations, systematic discrepancies from the QCD predicted values are observed in some conbinations; much higher in (a) $m = -2$ and in (c) the transverse moments, lower in (b) $m = +2$ and in (d) the longitudinal moments. Combinations of the mechanical moments or electric moments give the gluon fractions close to those obtained by 10 variables.

The discrepancies in gluon fractions between those obtained with positive and negative moments, and those with longitudinal and transverse moments indicate the difference in momentum spectra between the Monte Carlo generators and the CDF data. Soft (hard) charged particles contribute to the negative (positive) moments. Hence, if the momentum spectra of the Monte Carlo and the real data are different, one generally expect discrepancies in the gluon fractions. Likewise, a difference in the angular spread of charged particles results in the discrepancy in the gluon fractions obtained with the transverse and longitudinal moments. The sign of discrepancies shows that tracks in the CDF jets contain more softer and harder components and spread more than those in the Monte Carlo jets. Also, they are harder in the longitudinal moment distributions and softer in the transverse moment distributions than those in the Monte Carlo jets.

Symmetrical selection of the variables in the degrees of power and the number

of the transverse and longitudinal moments screens off the differences and makes it possible to study the quark/gluon likeliness of the CDF data with the QCD prediction by means of the Monte Carlo samples without a detailed tuning of each variables.

8 Conclusions

A comparison of the jet fragmentation properties of dijet and photon+jet processes in $\bar{p}p$ collisions at $\sqrt{s}$ =1.8 TeV has been made with the CDF data. We have shown that there is a difference in the charged particle multiplicity between jets from dijet and "γ"+jet events. The difference is consistent with that expected from the current QCD-based models of jet fragmentation.

We next performed a moment analysis of the momentum distributions of charged particles in the jet-rest frame. Various variables, i.e. mechanical/electric moments, multiplicity and EM fraction, are calculated for the CDF data and the reference quark and gluon jets generated by the Monte Carlo programs, PYTHIA and HERWIG . The moment distributions for the Monte Carlo generated jets suggest that gluon jets are softer and broader than quark jets, reflecting the larger color charge of the gluon. These reference jets were compared with CDF dijet events. Jets in the dijet samples show a strong preference for gluon-like behaviour. This is consistent with QCD predictions that the gluon jets are dominant at the low E_T range of the Tevatron ($\sqrt{s}$ =1.8 TeV).

We have taken a statistical approach to improve the separation power, i.e., each jet is characterized by a separation function which is a simple sum of all log-likelihood functions derived from 10 different variables. This results in a larger separation power than that of the most effective variable. The separation functions for dijet events show again that the dijet data are predominantly gluon rich, while "γ"+jet events are more

quark rich.

The gluon fraction in a given sample was determined by fitting its separation function distribution to the superposition of distributions from reference samples. The gluon fraction in dijet data shows a slight decrease with E_T and agrees with the QCD prediction. The "π^0"+jet data show a smaller gluon fraction than that in dijet data by 10 % to 30 % at E_T = 20 to 50 GeV. The gluon fraction of the "π^0"+jet data is higher than that of the "γ"+jet data by 10 % to 30 % at each E_T bin, which is consistent with the expectation from the QCD.

We also determined the gluon fraction using multiplicity only because of its large separation power in the entire E_T region. The results are mostly consistent with those obtained by the global likelihood/moment technique, but the uncertainties are larger. We also observed that symmetrical combination of moment variables can reduce the uncertainty in the moment analysis by canceling out differences in each variables between the Monte Carlo and the CDF data.

Acknowledgements

We thank the Fermilab staff and the technical staffs of the participating institutions for their vital contributions. This work was supported by the U.S. Department of Energy and National Science Foundation; the Italian Istituto Nazionale di Fisica Nucleare; the Ministry of Science, Culture, and Education of Japan; the Natural Sciences and Engineering Research Council of Canada; and the A. P. Sloan Foundation.

References

[1] JADE Collaboration, W. Bartel et al., Phys. Lett. B **123**, 460 (1983).

[2] H. Aihara et al., Z. Phys. C **28**, 31 (1985).

[3] AMY Collaboration, Y.K. Kim et. al., Phys. Rev. Lett. **63**, 1772 (1989).

[4] OPAL Collaboration, G. Alexander et al., Phys. Lett. B **265**, 462 (1991).

[5] M. Derrick et al., Phys. Lett. B **165**, 449 (1985).

[6] A. Petersen et al., Phys. Rev. Lett. **55**, 1954 (1985).

[7] TASSO Collaboration, M. Althoff et al., Z. Phys. C **22**, 307 (1984);
W. Braunschweig et al., DESY Report DESY 89-032 (1989).

[8] UA1 Collaboration, G. Arnison et al., Nucl. Phys. B **276**, 253 (1986);
P. Ghez and G. Ingelman, Z. Phys. C **33**, 465 (1987).

[9] L.M. Jones, Phys. Rev. D **39**, 2550 (1989);
L.M. Jones, Phys. Rev. D **42**, 811 (1990).

[10] S. Wolfram, in Proc. 15th Rencontre de Moriond (1980), ed. J.Tran Thanh Van;
G.C. Fox and S. Wolfram, Nucl. Phys. B **168**, 285 (1980);
R.D. Field and S. Wolfram, Nucl. Phys. B **213**, 65 (1983).

[11] T.D. Gottschalk, Nucl. Phys. B **214**, 201 (1983); B **227**, 413 (1983);
T.D. Gottschalk, in Proc. UCLA workshop on SSC physics (1986).

[12] G. Marchesini and B.R. Webber, Nucl. Phys. B **238**, 1 (1984);
B.R. Webber, Nucl. Phys. B **238**, 492 (1984).

[13] B. Andersson, G. Gustafson and C. Peterson, Z. Phys. C **1**, 105(1979);
B. Andersson, G. Gustafson and B. Söderberg, Z. Phys. C **20**, 317 (1983).

[14] G. Marchesini, B.R. Webber, et al. Computer Phys. Comm. **67**, 465 (1992).

[15] H.-U. Bengtsson and T. Sjöstrand, Computer Phys. Comm. **46**, 43 (1987).

[16] T. Sjöstrand , Computer Phys. Comm. **39**, 347 (1986).

[17] CDF Collaboration, F. Abe et al., Nucl. Instr. and Meth. A **271**, 387 (1988).

[18] CDF Collaboration, F.Abe et al., Phys. Rev. Lett. **65**, 968 (1990).

[19] CDF Collaboration, F. Abe et al., Phys. Rev. Lett. **68**, 1104 (1992).

[20] CDF Collaboration, F. Abe et al., Phys. Rev. Lett. **62**, 613 (1989).

[21] CDF Collaboration, F. Abe et al., Phys. Rev. Lett. **68**, 2734 (1992);
Phys. Rev. D **48**, 2998 (1993).

[22] CDF Collaboration, F.Abe et al., Phys. Rev. D. **43**, 664 (1991).

[23] F. Paige and S. Protopopescu, ISAJET Monte Carlo program Version 6.21, BNL Report No.BNL38034 (1986)

[24] S.J. Brodsky and J.F. Gunion, Phys. Rev. Lett. **37**, 402 (1976).

[25] K. Konishi, A. Ukawa and G. Veneziano, Nucl. Phys. B **157**, 45 (1979).

[26] A. Bassetto, M.M. Ciafani and G. Marchesini, Nucl. Phys. B **163**, 477 (1980).

[27] Y.L. Dokshitzer, V.S. Fadin and V.A. Khoze, Phys. Lett. B **115**, 242 (1982);
Z.Phys. C **15**, 325(1982); C **18**, 408 (1983).

[28] A.H. Mueller, Nucl. Phys. B **241**, 141 (1984);
J.B. Gaffney and A.H. Mueller Nucl. Phys. B**250**, 109 (1985).

[29] S. Kanda, S. Kim, and K. Kondo, Computer Phys. Comm. **67**, 223 (1991);

[30] S. Kanda, Ph.D. Thesis, University of Tsukuba, 1990 (unpublished)

[31] CDF Collaboration., F. Abe et al., Phys. Rev. D. **45**, 1448 (1992).

[32] M. Ninomiya, Ph.D. Thesis, University of Tsukuba, 1992 (unpublished)

[33] A. Martin, R. Roberts and W. Stirling, Phys. Rev. D. **47**, 867 (1993); Phys. Lett. **306B**, 145 (1993), Phys. Lett. **309B**, 492 (1993).

[34] H. Plothow-Besch, CERN-PPE W5051 PDFLIB (1993) ver.4.00

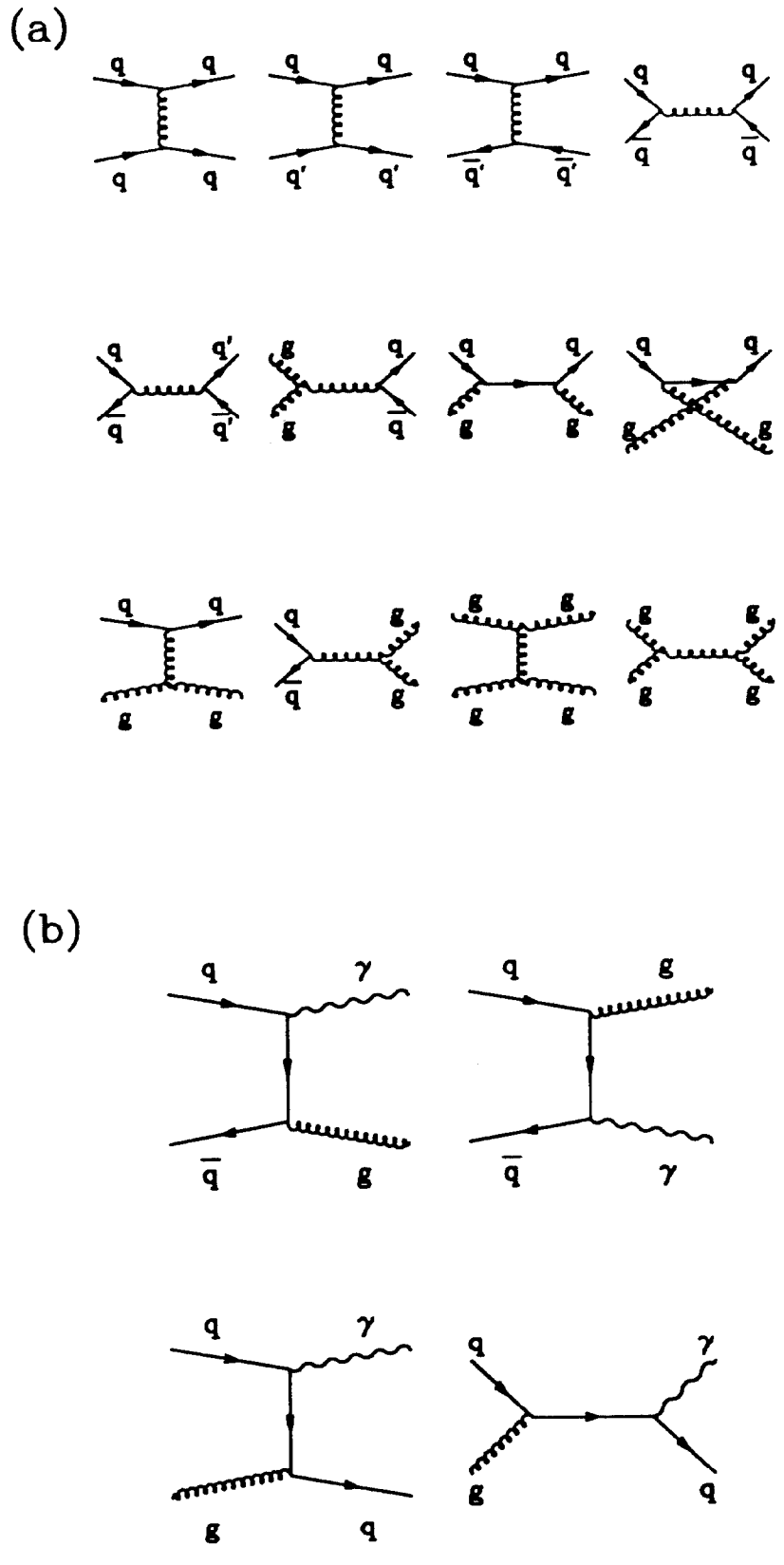

Figure 1: The lowest order Feynman graphs for (a) the dijet processes, and (b) the γ+jet processes.

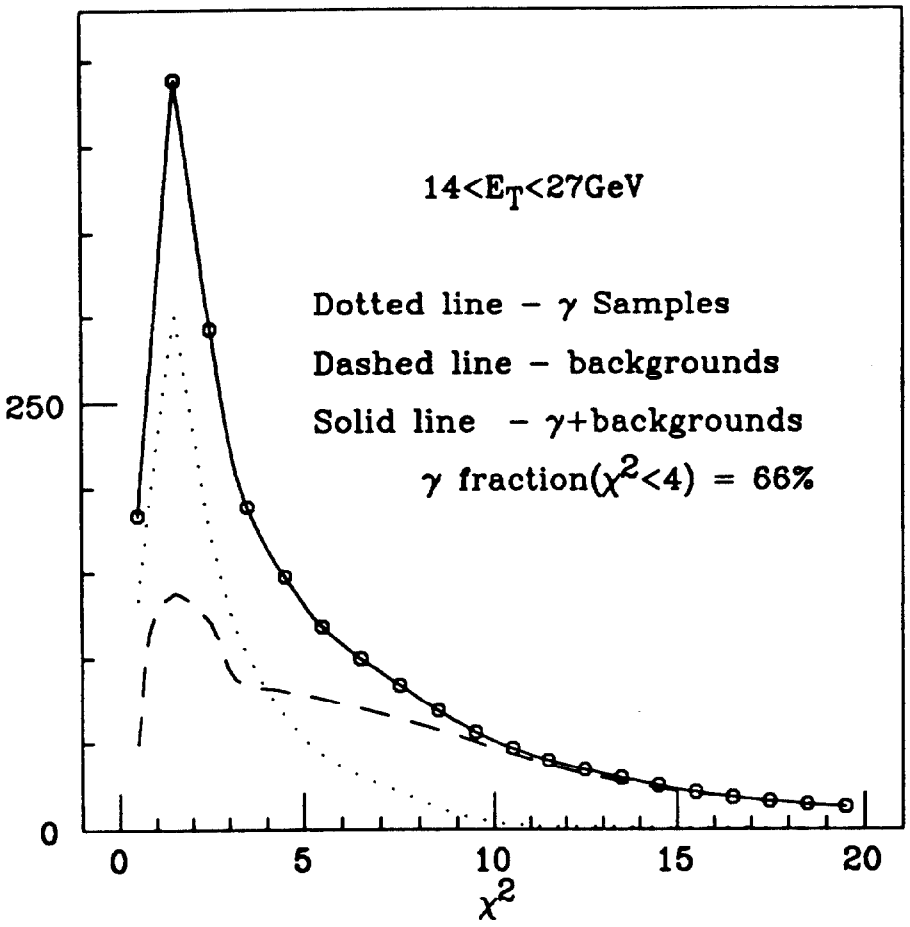

Figure 2: The average χ^2 for the central strip chamber profiles, which represents the single photon likelihood, is shown by the dotted line and the dashed line for the simulated photon(s) events and the backgrounds (π^0, η and K_s), respectively. The solid line and points show the distributions for the sum of simulated photons and backgrounds. The E_T range is 14 – 27 GeV[21].

dijet

E_T(GeV)	10 – 20	20 – 30	30 – 40	40 – 50	50 – 60	60 – 70	70 – 80	80 – 90
	2102	3693	4145	6506	3712	4476	3141	1506

"γ"+jet

E_T(GeV)	10 – 20	20 – 30	30 – 40	40 – 50
	376	602	493	188

"π^0"+jet

E_T(GeV)	10 – 20	20 – 30	30 – 40	40 – 50
	434	597	357	160

Table 1: The number of analyzed jets in the CDF data for dijet, "γ"+jet and "π^0"+jet processes. The number of jets in the dijet process has the maximum value at E_T = 40 – 50 GeV, which is related to the corrected trigger E_T threshold of leading jets for two trigger samples. It is about 30 GeV for the lower trigger E_T sample and 50 GeV for the higher trigger E_T sample. Since the prescale factor of the latter sample is ten times smaller than that of the former sample, the decrease of the number of jets with E_T is rather unclear in the E_T range of 30 – 80 GeV. This is also seen in "γ/π^0"+jet sample, where the integrated luminosity of the lower trigger sample (10 GeV) was only about 3 % of the higher trigger sample (23 GeV).

E_T (GeV)	PYTHIA Monte Carlo			
	gluon		quark	
	mean	variance	mean	variance
10 – 20	5.48±0.03	2.08	4.55±0.02	1.79
20 – 30	6.67±0.03	2.49	5.13±0.03	2.14
30 – 40	7.63±0.04	2.90	5.57±0.03	2.43
40 – 50	8.34±0.04	3.22	5.85±0.04	2.71
50 – 60	8.77±0.05	3.45	6.09±0.04	2.88
60 – 70	9.18±0.05	3.74	6.35±0.04	3.04
70 – 80	9.40±0.05	3.81	6.48±0.04	3.20
80 – 90	9.62±0.05	4.01	6.55±0.04	3.21

E_T (GeV)	CDF data			
	dijet		"γ"+jet	
	mean	variance	mean	variance
10 – 20	5.57±0.05	2.14	5.39±0.10	2.01
20 – 30	6.63±0.04	2.61	6.32±0.10	2.53
30 – 40	7.26±0.05	2.91	6.72±0.12	2.73
40 – 50	7.55±0.04	3.10	7.15±0.23	3.12
50 – 60	8.20±0.06	3.46		
60 – 70	8.20±0.05	3.58		
70 – 80	8.59±0.07	3.75		
80 – 90	8.79±0.10	3.83		

Table 2: Mean values and variances of the charged multiplicity for PYTHIA Monte Carlo gluon- and quark-jet, CDF dijet and "γ"+jet events.

Variables #	Moment definition
1	$\sum(k_{Ti}/M)^{-2}$
2	$\sum(k_{Ti}/M)^{2}$
3	$\sum Q_i(k_{Ti}/M)^{-2}$
4	$\sum Q_i(k_{Ti}/M)^{2}$
5	$E_T(EM)/E_T(TOTAL)$
6	multiplicity
7	$\sum(k_{Li}/M)^{-2}$
8	$\sum(k_{Li}/M)^{2}$
9	$\sum Q_i(k_{Li}/M)^{-2}$
10	$\sum Q_i(k_{Li}/M)^{2}$

Table 3: The momnet variables used in the analysis.

Variables #	S.P.(PYTHIA)	S.P.(HERWIG)
1	0.62	0.51
2	0.26	0.25
3	0.45	0.37
4	0.23	0.27
5	0.28	0.27
6	0.79	0.63
7	0.57	0.50
8	0.42	0.40
9	0.49	0.42
10	0.39	0.39

Table 4: The separation powers (S.P.) of the 10 variables used in this analysis, for simulated jets with E_T from 30 to 40 GeV, are listed for two kinds of Monte Carlo generators (PYTHIA, HERWIG). The variable ID corresponds to that in Table 3. Statistical errors are $\pm$ 0.03 for all variables.

E_T(GeV)	10 – 20	20 – 30	30 – 40	40 – 50	50 – 60	60 – 70	70 – 80	80 – 90
(1) (%)	−3.8	−3.4	−3.4	−3.4	−3.8	−3.9	−4.1	−4.7
(2) (%)	−3.0	−3.2	−3.4	−3.3	−3.4	−3.4	−3.7	−3.6
(3) (%)	10.3	8.4	10.8	9.4	5.0	7.1	2.1	3.6
(4) (%)	6.7	4.3	5.4	7.1	9.0	13.3	9.6	14.8
(5) (%)	+8.6	+6.4	+7.6	+8.8	+10.6	+14.4	+11.3	+16.3
	−12.5	−9.5	−12.3	−12.0	−10.5	−15.2	−10.1	−15.6
(6) (%)	+13.8	+10.8	+13.2	+12.8	+11.7	+16.1	+11.5	+16.6
	−7.8	−4.9	−5.8	−7.3	−9.2	−13.5	−9.9	−15.1
(7) (%)	0.1	1.1	1.2	1.3	2.2	1.4	1.8	1.8

Table 5: The systematic uncertainties in the gluon fraction of dijet process as a function of E_T due to (1) the difference in the needed energy correction for quark and gluon jets, (2) the discrepancy of the E_T spectrum from the real data in the energy correction, (3) the difference of the referenced Monte Carlo generators (HERWIG to PYTHIA) and (4) an uncertainty of the track finding efficiency. The quadratic sum of the systematic and statistical uncertainties for the gluon fraction found by using (5) HERWIG and (6) PYTHIA are also listed as a function of E_T. Theoretical uncertainty in the gluon fraction due to the difference of the structure functions of MRS D'_0 and D'_- is also shown as a function of E_T in the line of (7).

E_T(GeV)	10 – 20	20 – 30	30 – 40	40 – 50
Gluon	0.158±0.006	0.240±0.008	0.399±0.010	0.446±0.011
Quark	0.225±0.007	0.361±0.007	0.437±0.008	0.482±0.009
E_T(GeV)	50 – 60	60 – 70	70 – 80	80 – 90
Gluon	0.494±0.012	0.515±0.013	0.561±0.015	0.560±0.015
Quark	0.520±0.010	0.526±0.010	0.542±0.011	0.537±0.011

Table 6: The overall acceptance for quark and gluon dijet processes as a function of E_T. The errors are from the statistics of the Monte Carlo.

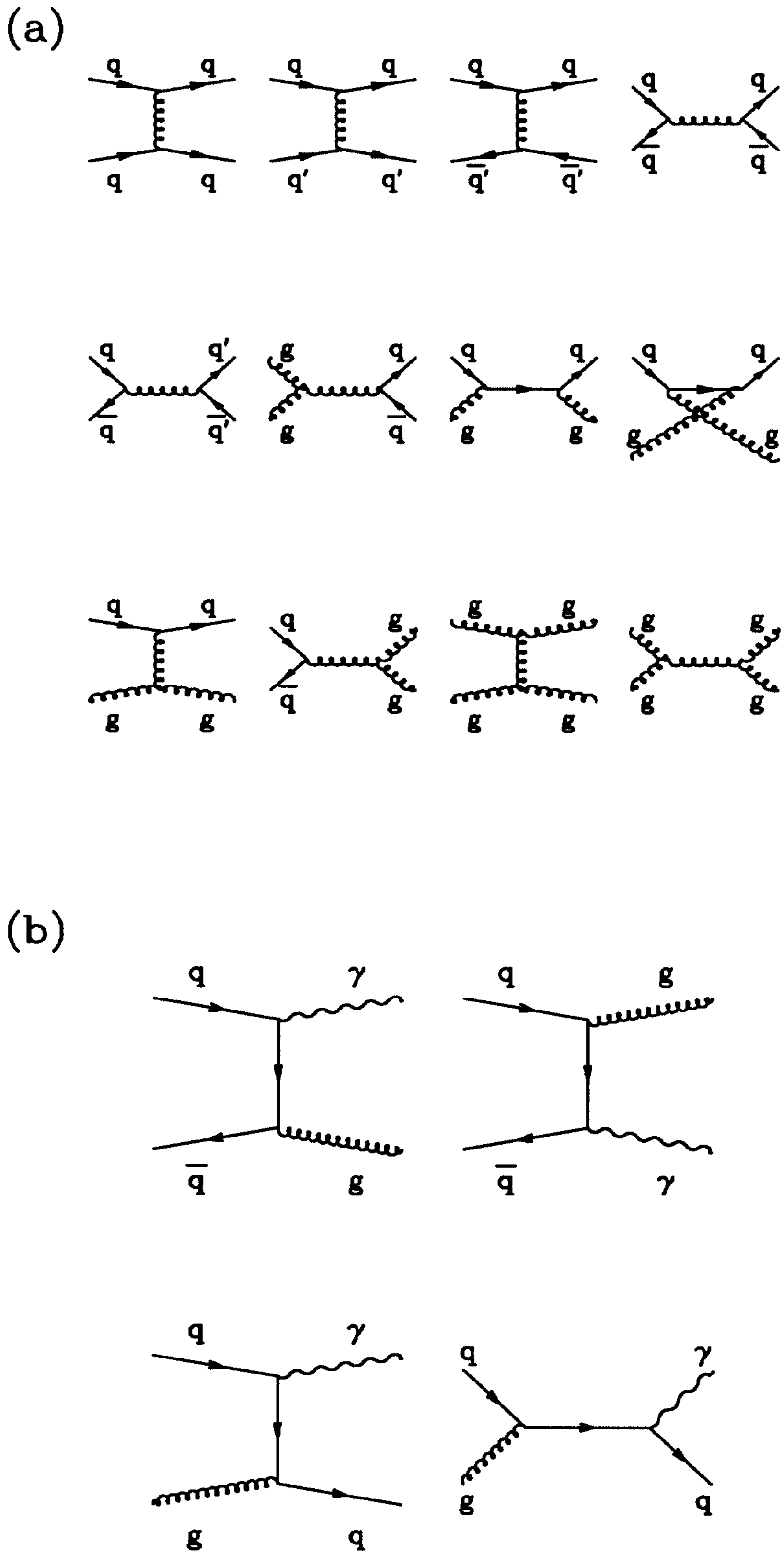

Figure 1: The lowest order Feynman graphs for (a) the dijet processes, and (b) the γ+jet processes.

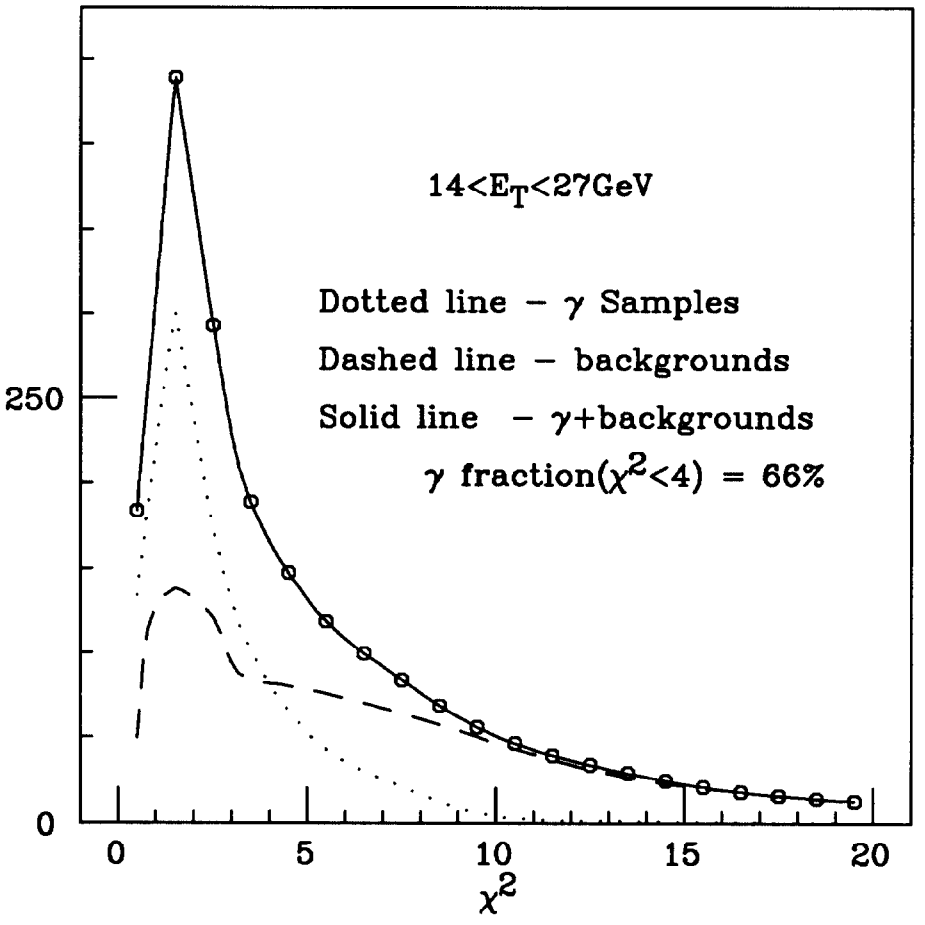

Figure 2: The average χ^2 for the central strip chamber profiles, which represents the single photon likelihood, is shown by the dotted line and the dashed line for the simulated photon(s) events and the backgrounds (π^0, η and K_s), respectively. The solid line and points show the distributions for the sum of simulated photons and backgrounds. The E_T range is $14 - 27$ GeV[21].

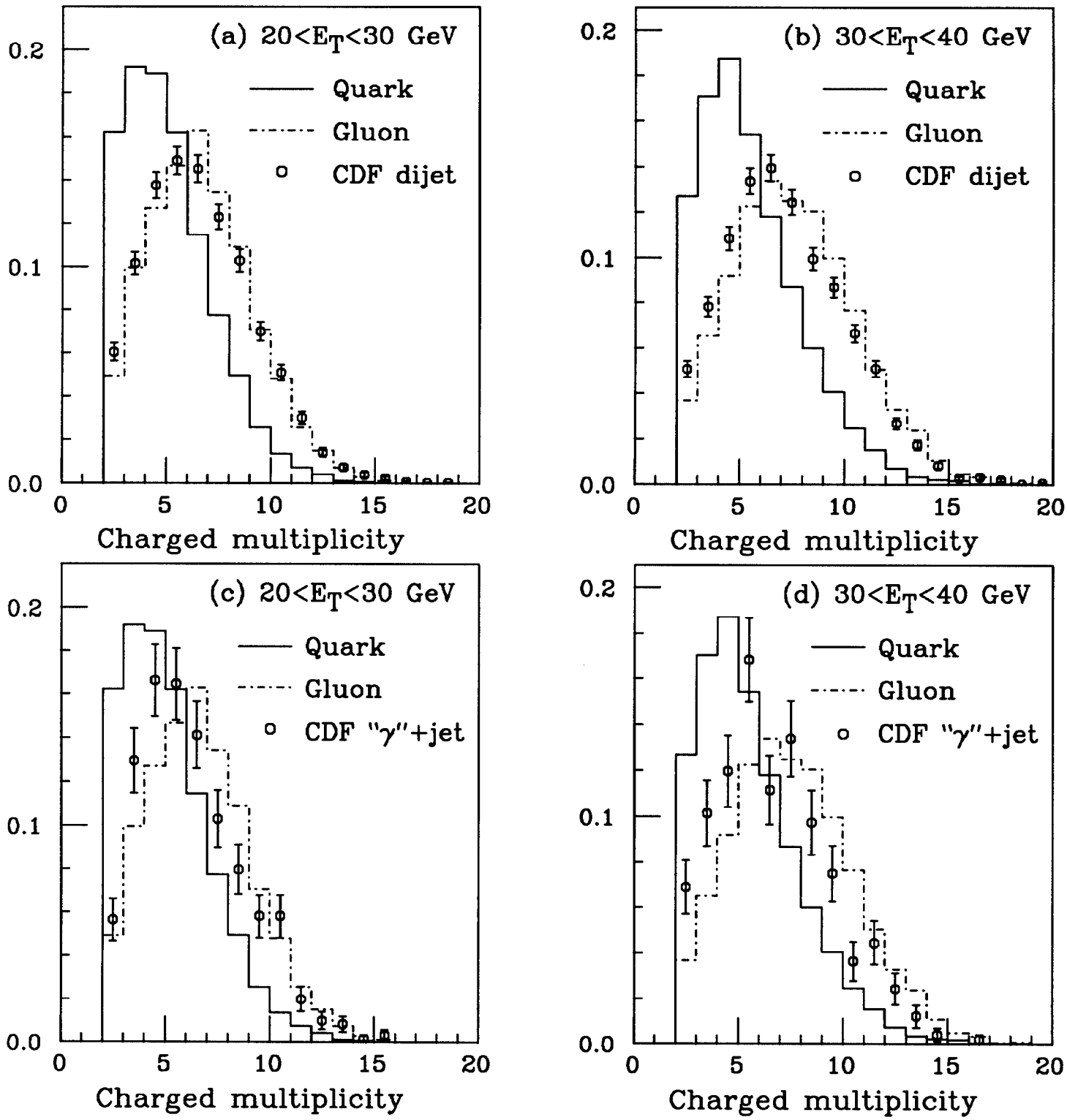
(a) 20<E_T<30 GeV
Quark
Gluon
CDF dijet
(b) 30<E_T<40 GeV
Quark
Gluon
CDF dijet
(c) 20<E_T<30 GeV
Quark
Gluon
CDF "γ"+jet
(d) 30<E_T<40 GeV
Quark
Gluon
CDF "γ"+jet
0.0
0.1
0.2
0
5
10
15
20
Charged multiplicity

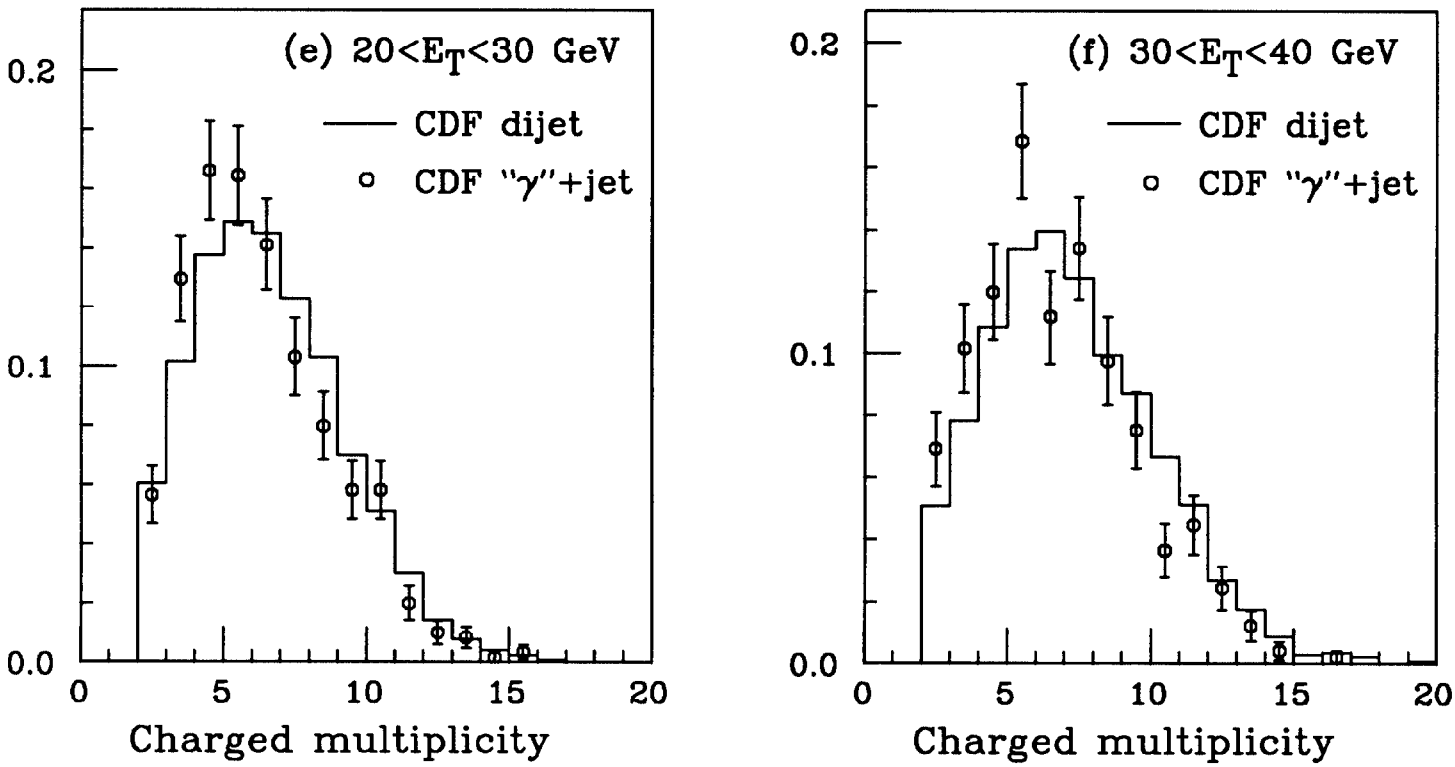

Figure 3: Distributions of jet charged multiplicity. The multiplicities for quark and gluon jets generated by PYTHIA Monte Carlo program are compared with those for CDF jets in (a) to (d). The open circles in (a) to (d) represent the observed multiplicities for the dijet and "γ"+jet processes. In (e) and (f), multiplicities for the CDF dijet events(solid lines) are compared with those for the CDF "γ"+jet events(open circles). The E_T range of jets is 20−30 GeV in (a), (c) and (e), and is 30−40 GeV in (b), (d) and (f).

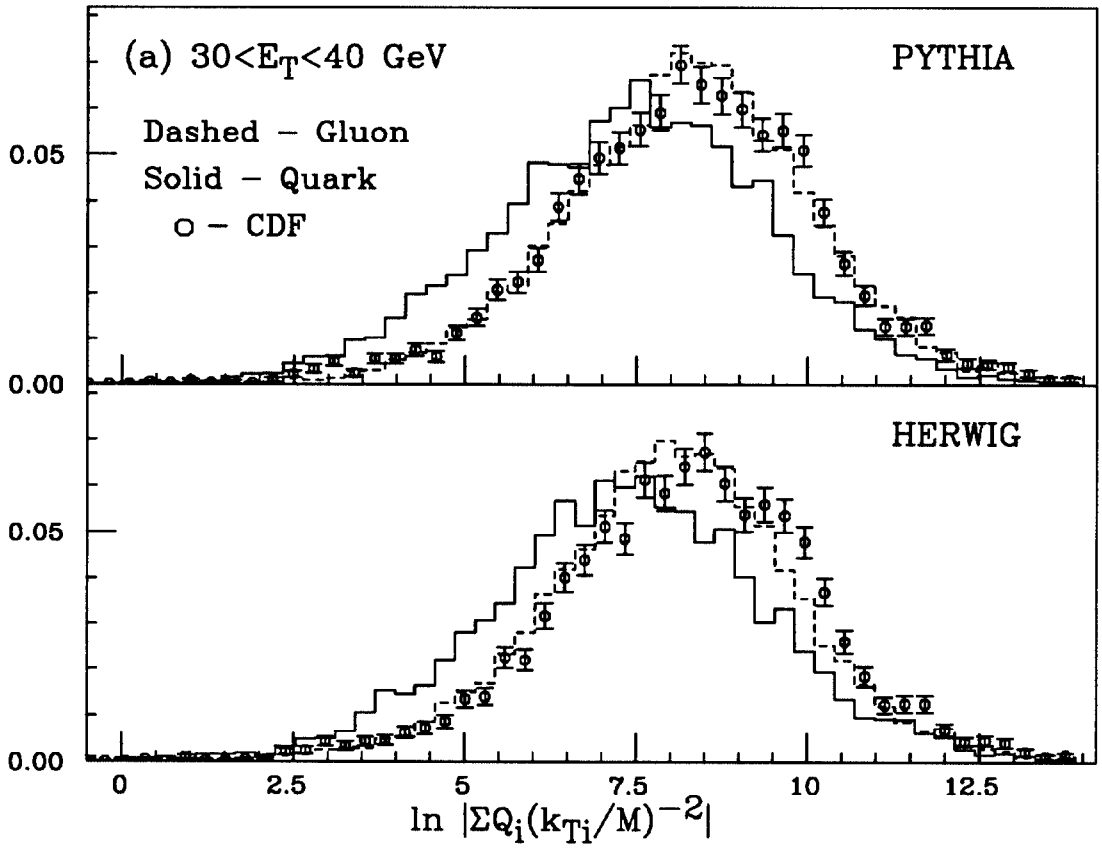
(a) 30<E_T<40 GeV
PYTHIA
Dashed – Gluon
Solid – Quark
o – CDF
HERWIG
0.05
0.00
0.05
0.00
0
2.5
5
7.5
10
12.5
ln |ΣQ_i(k_Ti/M)^-2|

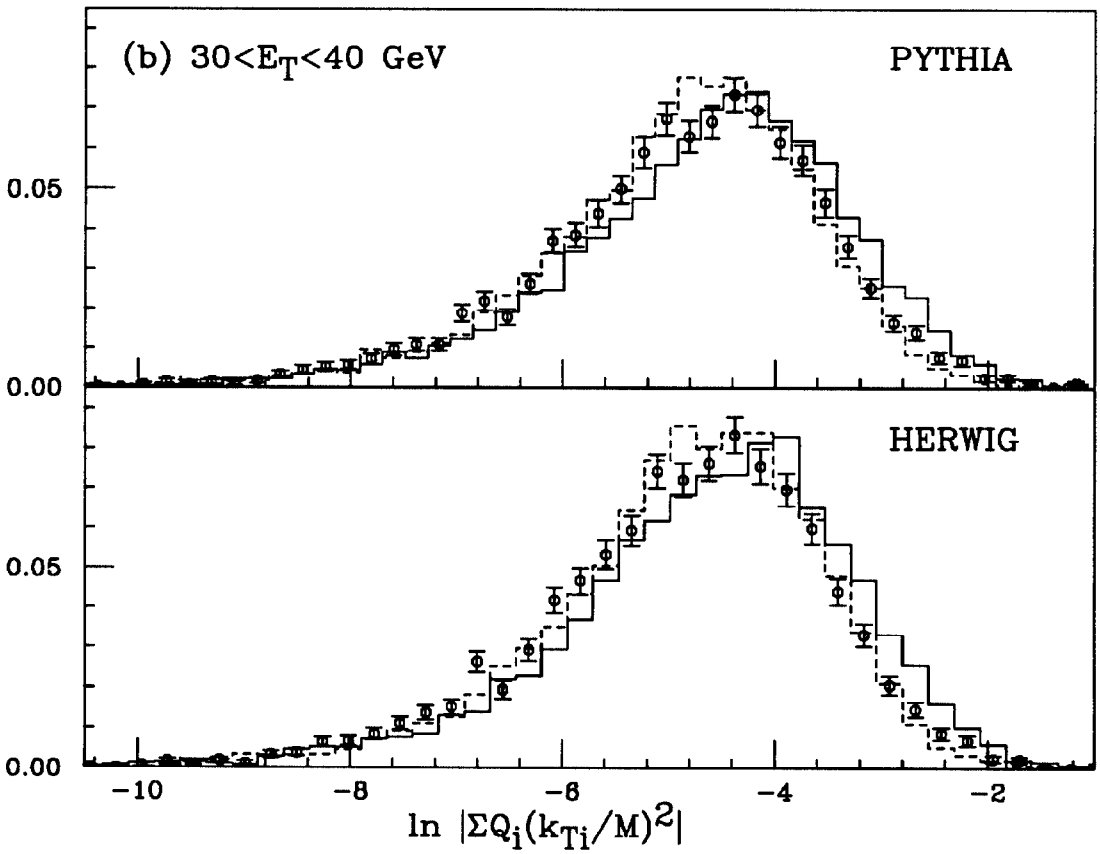
(b) 30<E_T<40 GeV
PYTHIA
HERWIG
0.05
0.00
0.05
0.00
−10
−8
−6
−4
−2
ln |ΣQ_i(k_Ti/M)^2|

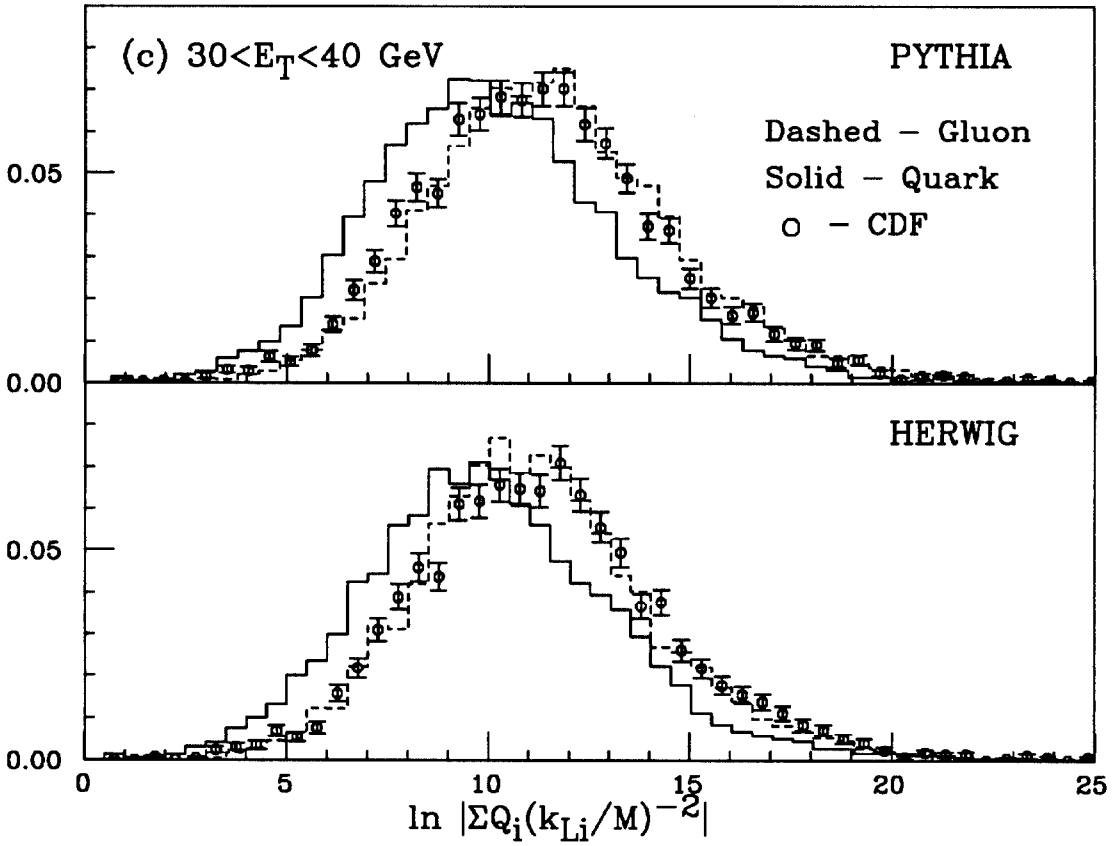
(c) 30<E_T<40 GeV
PYTHIA
Dashed – Gluon
Solid – Quark
o – CDF
HERWIG
0.05
0.00
0.05
0.00
0
5
10
15
20
25
ln |ΣQ_i(k_Li/M)^-2|

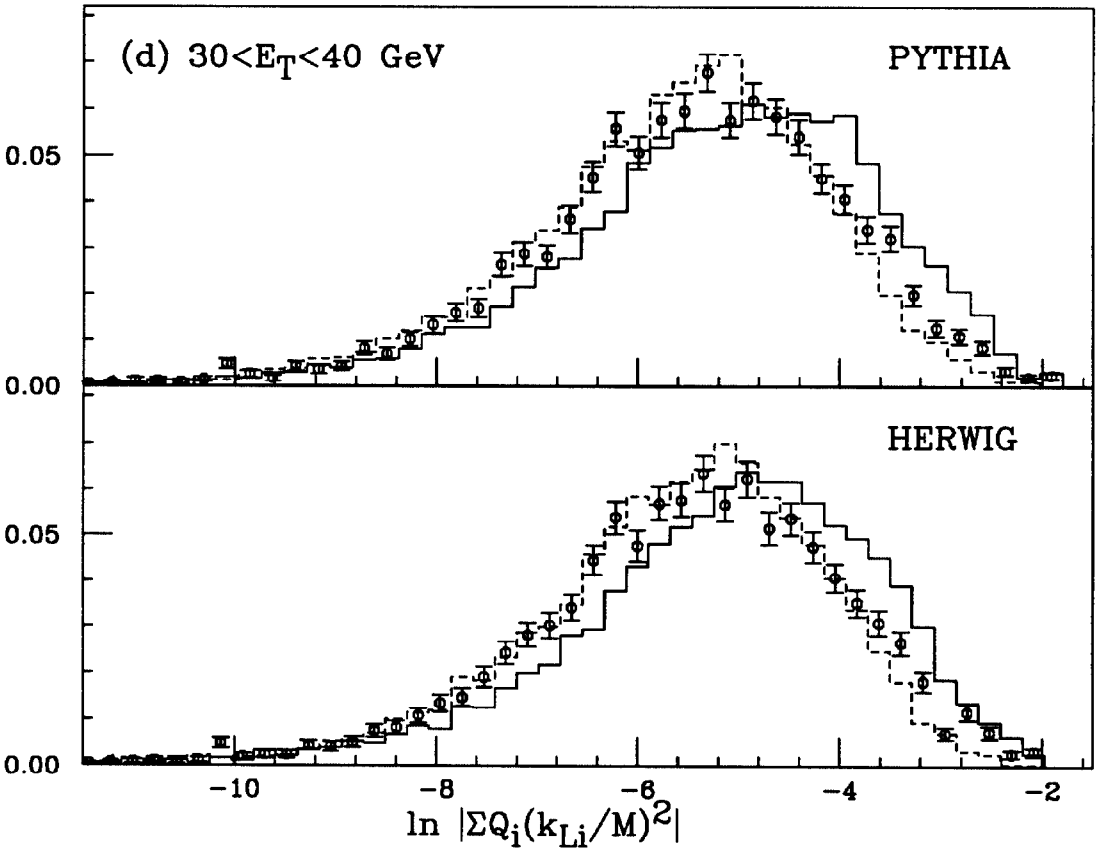
(d) 30<E_T<40 GeV
PYTHIA
HERWIG
0.05
0.00
0.05
0.00
−10
−8
−6
−4
−2
ln |ΣQ_i(k_Li/M)^2|

Figure 4: Distributions of moments for $30 < E_T < 40GeV$: (a) $\ln|\sum Q_i(k_{Ti}/M)^{-2}|$, (b) $\ln|\sum Q_i(k_{Ti}/M)^2|$, (c) $\ln|\sum Q_i(k_{Li}/M)^{-2}|$ and (d) $\ln|\sum Q_i(k_{Li}/M)^2|$, where the sum is over charged tracks(i) associated with a jet, subscripts L and T stand for moments for the longitudinal and transverse momentum components with respect to the jet axis, Q_i is the charge of the i-th particle, and M is the jet invariant mass. The solid lines show the moment distribution for quark jets, the dashed lines gluon jets and the open circles CDF dijet data. The quark and gluon jets were produced with PYTHIA and HERWIG Monte Carlo programs and a CDF detector simulation.

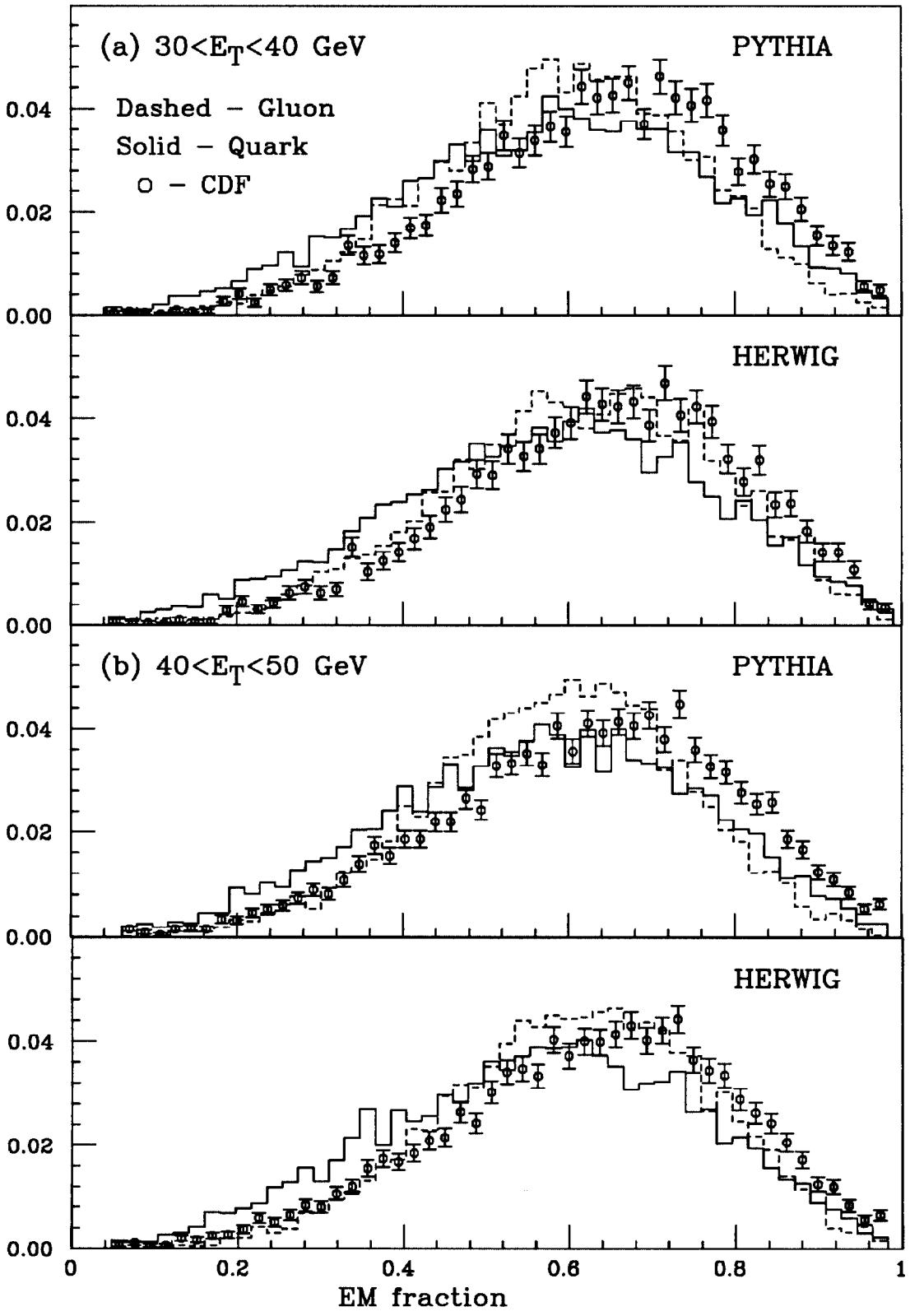

Figure 5: Distributions of the electromagnetic energy fraction of jets. Solid lines are for quark jets, dashed lines are for gluon jets, and open circles represent CDF dijet data. The E_T range of jets is 30–40 GeV in (a) and 40–50 GeV in (b).

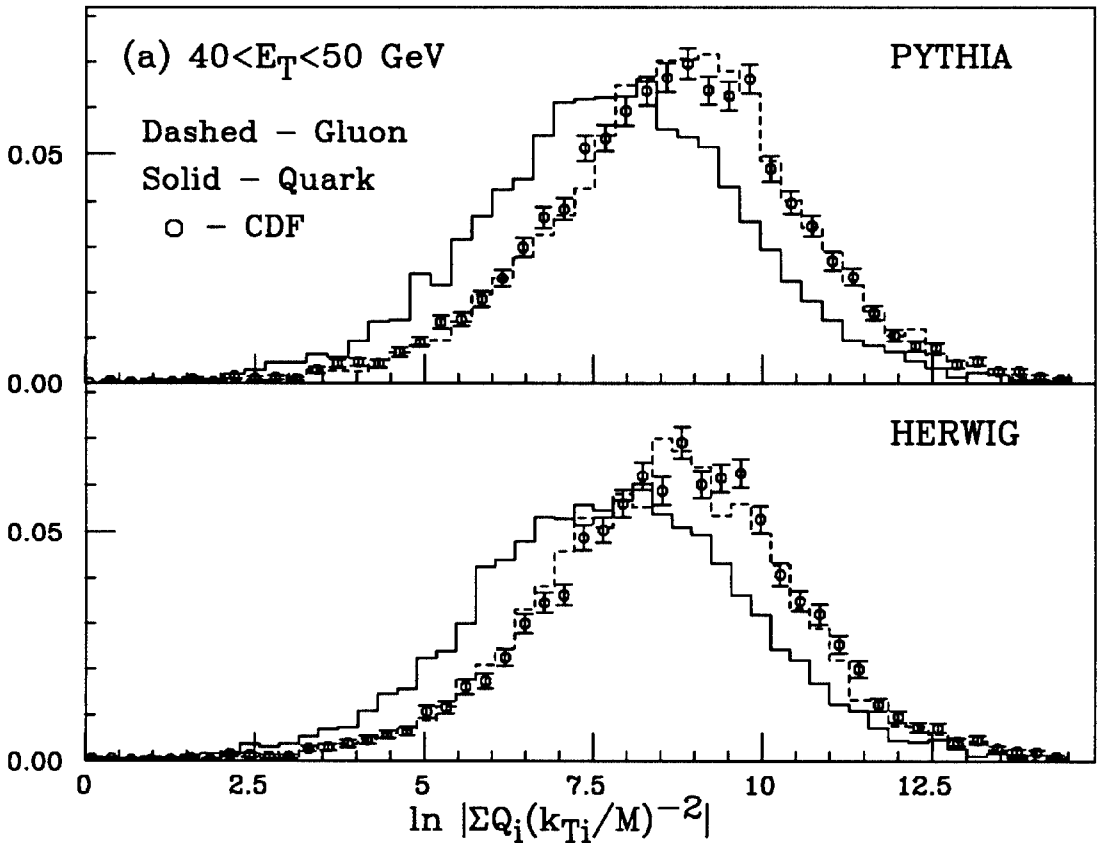
(a) 40<E_T<50 GeV
PYTHIA
Dashed – Gluon
Solid – Quark
o – CDF
HERWIG
0.05
0.00
0.05
0.00
0
2.5
5
7.5
10
12.5
ln |ΣQ_i(k_Ti/M)^-2|

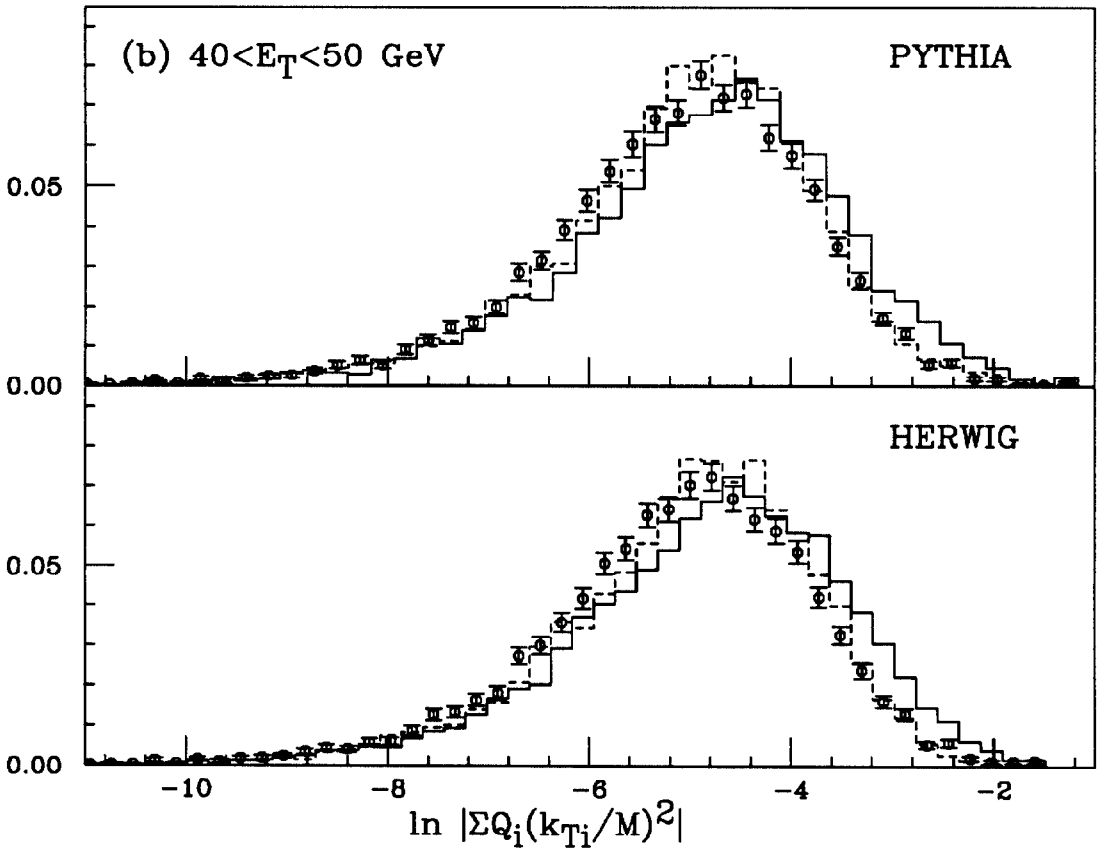
(b) 40<E_T<50 GeV
PYTHIA
HERWIG
0.05
0.00
0.05
0.00
−10
−8
−6
−4
−2
ln |ΣQ_i(k_Ti/M)^2|

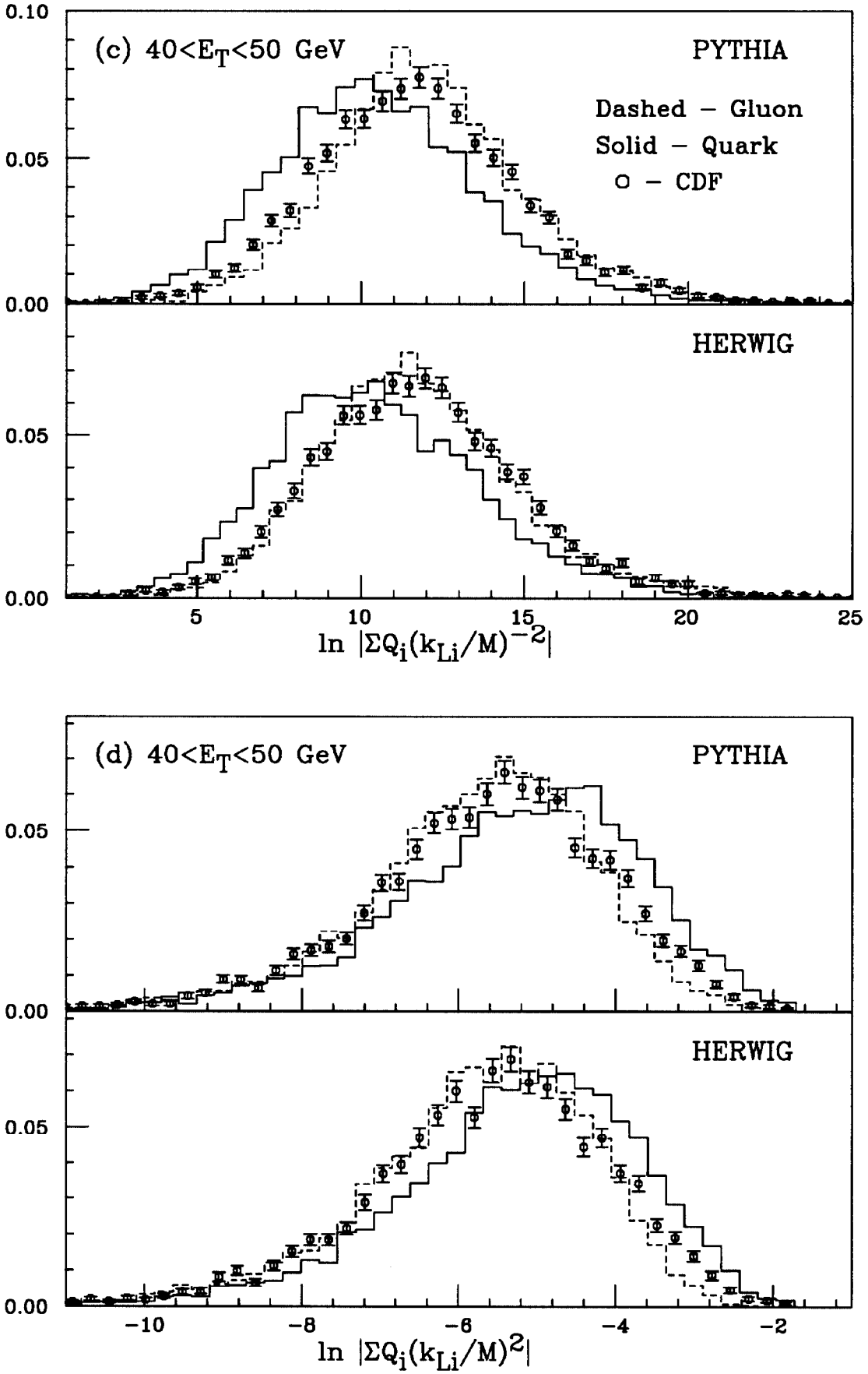

Figure 6: Distributions of moments as described in Figure 4 for $40 < E_T < 50 GeV$.

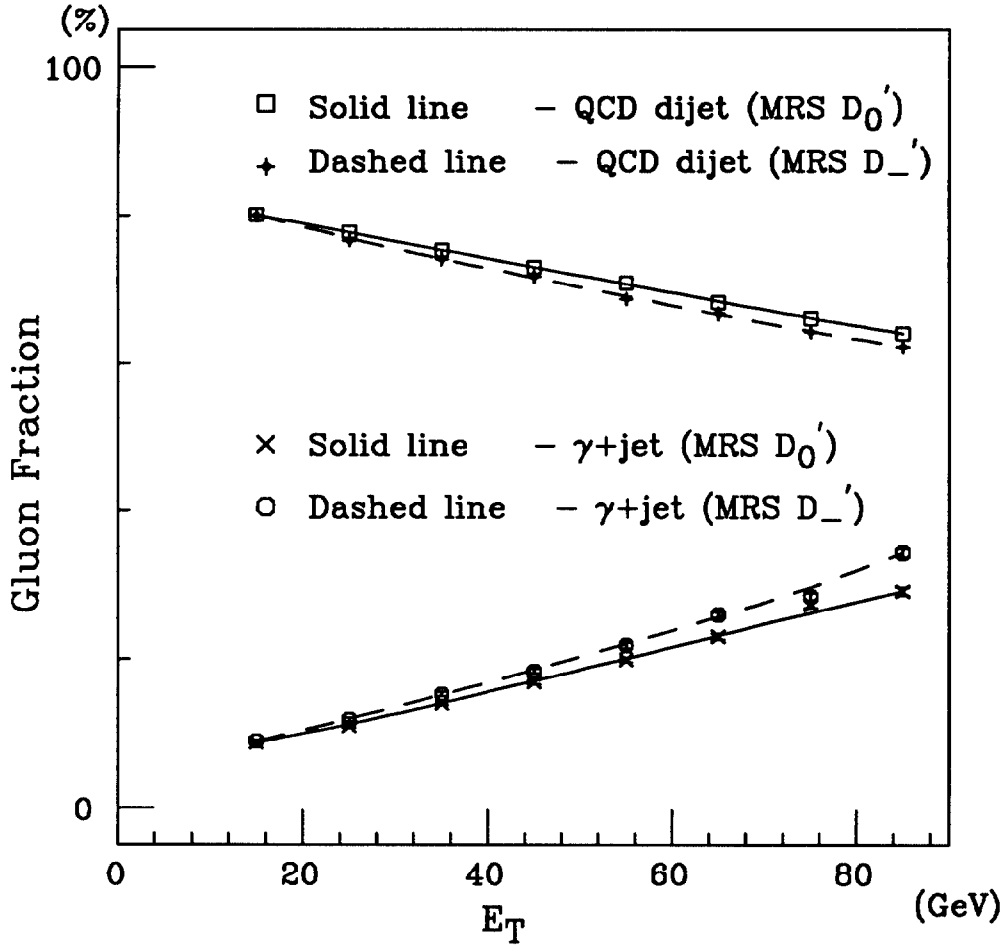

Figure 7: The gluon jet fraction for jets with $|\eta| < 0.7$ obtained from sub-process cross sections for the QCD dijet and γ+jet processes, as a function of jet transverse energy (E_T). The PYTHIA Monte Carlo programs and a library of parton density functions[34] are used with structure functions by MRS D_0' and D_-' [33] using the QCD scale parameter $\Lambda_{QCD}(N_f = 4) = 215$ MeV. Lines are drawn to guide the eye by a smooth fit through the data.

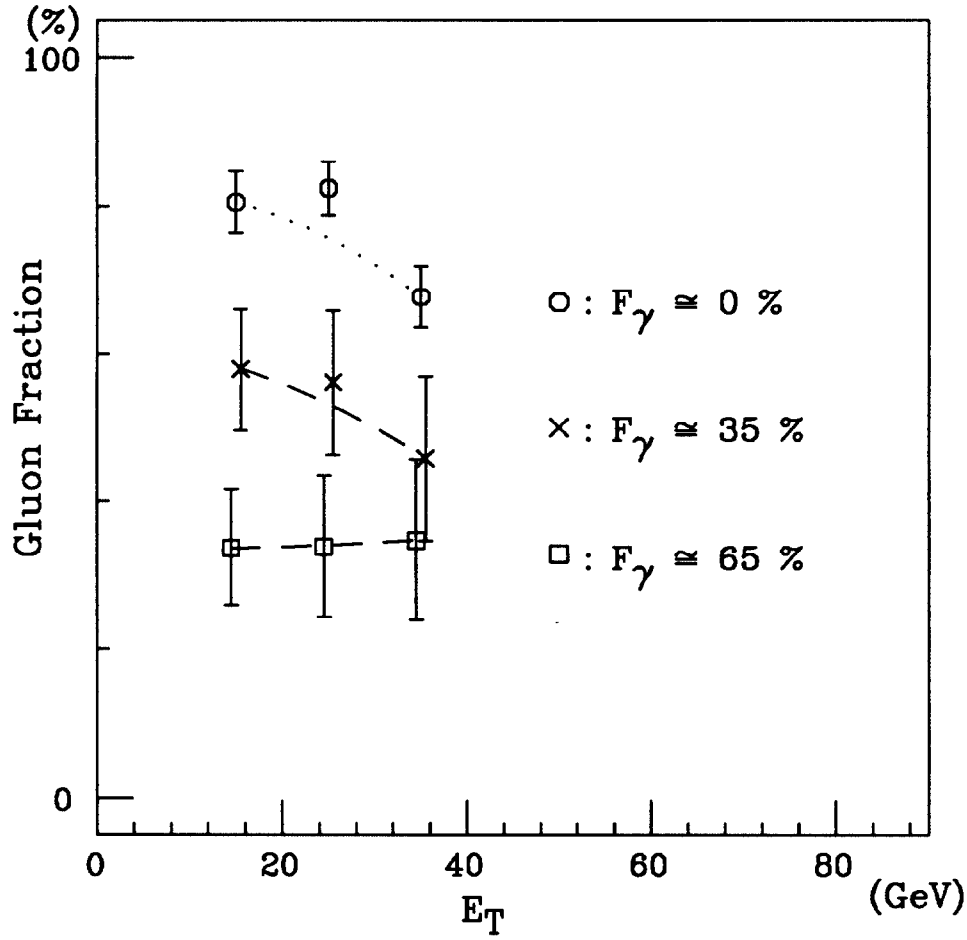

Figure 8: The gluon fraction in the HERWIG Monte Carlo QCD dijet samples which passed the event selection cuts for the real photon+jet data are shown as a function of E_T of the jet by open circles. The expected gluon fractions given in Eq. (3) for the CDF "π^0"+jet and "γ"+jet events are also shown by cross and square points, respectively. Dotted and dashed lines are drawn to guide the eye by a smooth fit through the data.

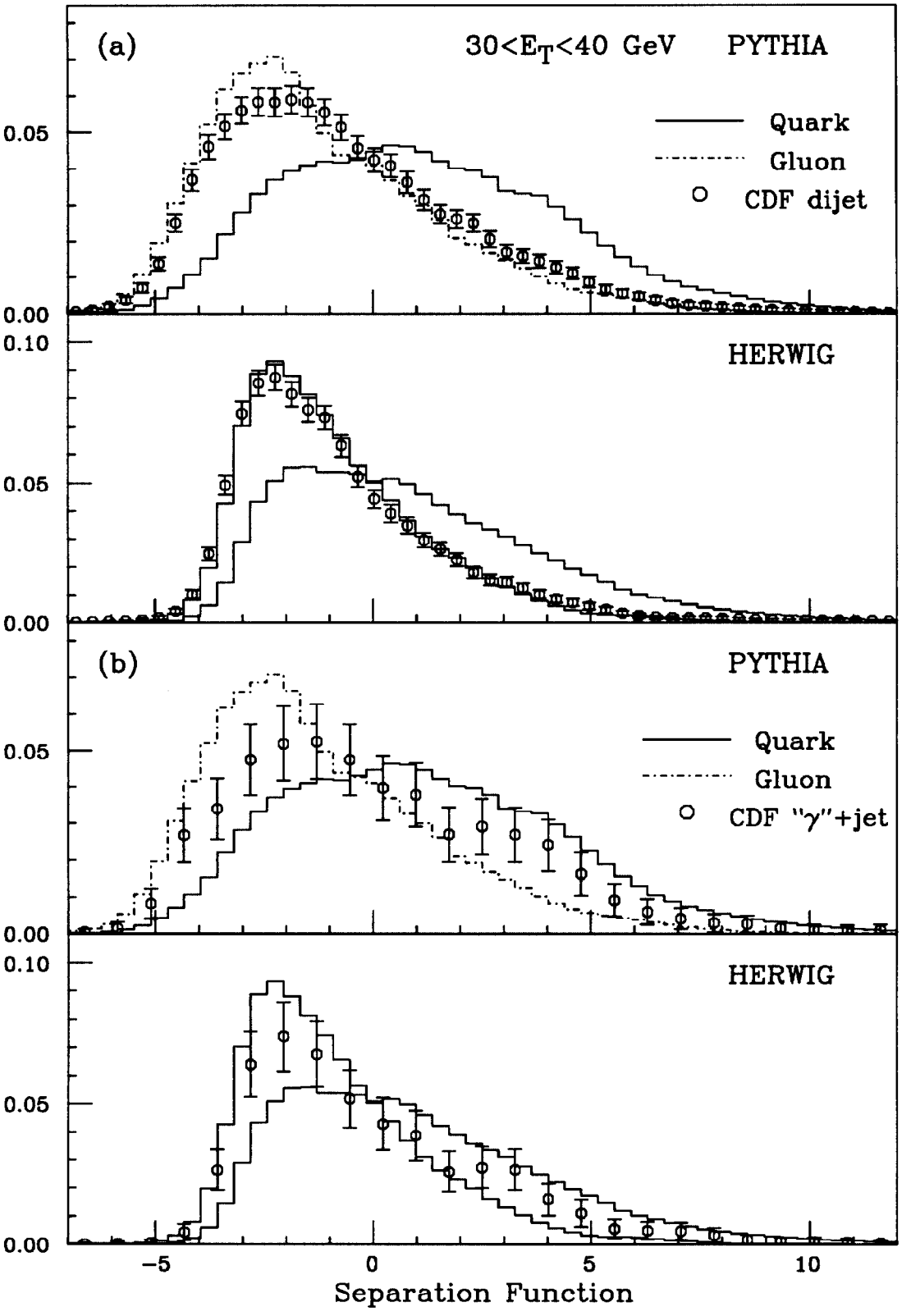
(a)
30<E_T<40 GeV
PYTHIA
Quark
Gluon
CDF dijet
HERWIG
(b)
PYTHIA
Quark
Gluon
CDF "γ"+jet
HERWIG
0.00
0.05
0.10
−5
0
5
10
Separation Function

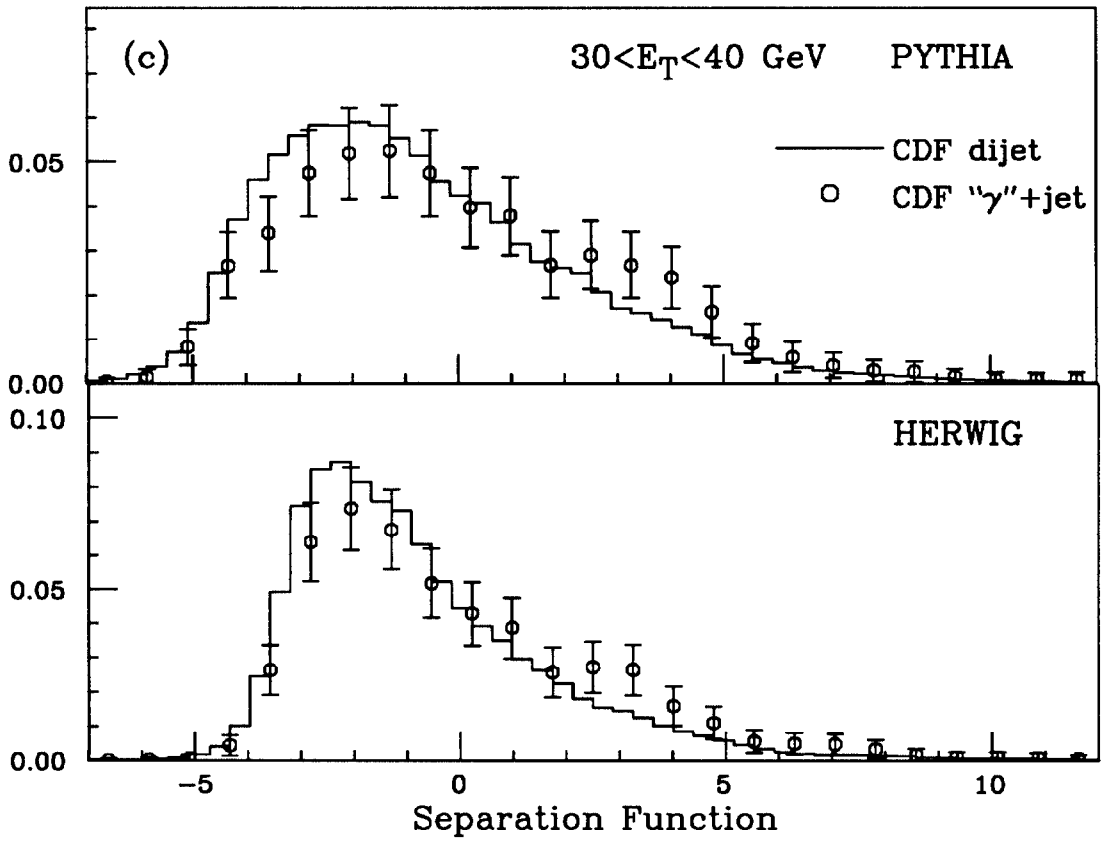

Figure 9: In (a) and (b), separation function distributions for simulated jets generated with the PYTHIA and HERWIG Monte Carlo programs are compared with those for CDF jet data in the range $30 < E_T < 40$ GeV. Open circles in (a) show the CDF dijet data, and those in (b) the CDF "γ"+jet data, respectively. In (c), the CDF dijet data(solid lines) are compared with the CDF "γ"+jet data(open circles).

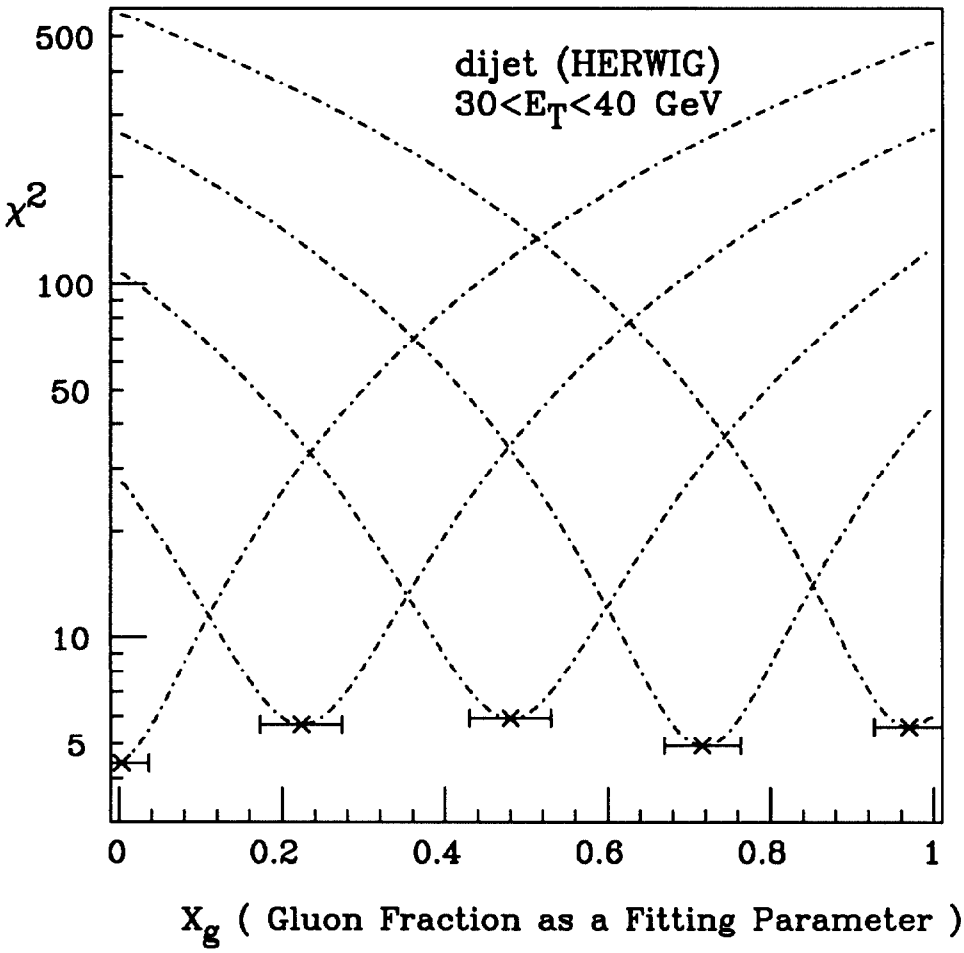

Figure 10: χ^2 found by Eq. (9) versus the fitting parameter X_g at E_T = 30–40 GeV. Referenced and analyzed jets are identical with those used in Fig. 11. Each line in the figure coresponds to the ratio of gluon jets in the analyzed sample of 0%, 25%, 50%, 75% and 100% from left to right, respectively. X_g at the minimum value of χ^2(χ^2_{min}) is used to estimate the gluon fraction in the analyzed sample. The errors are obtained from a condition $\chi^2 = \chi^2_{min} + 1$.

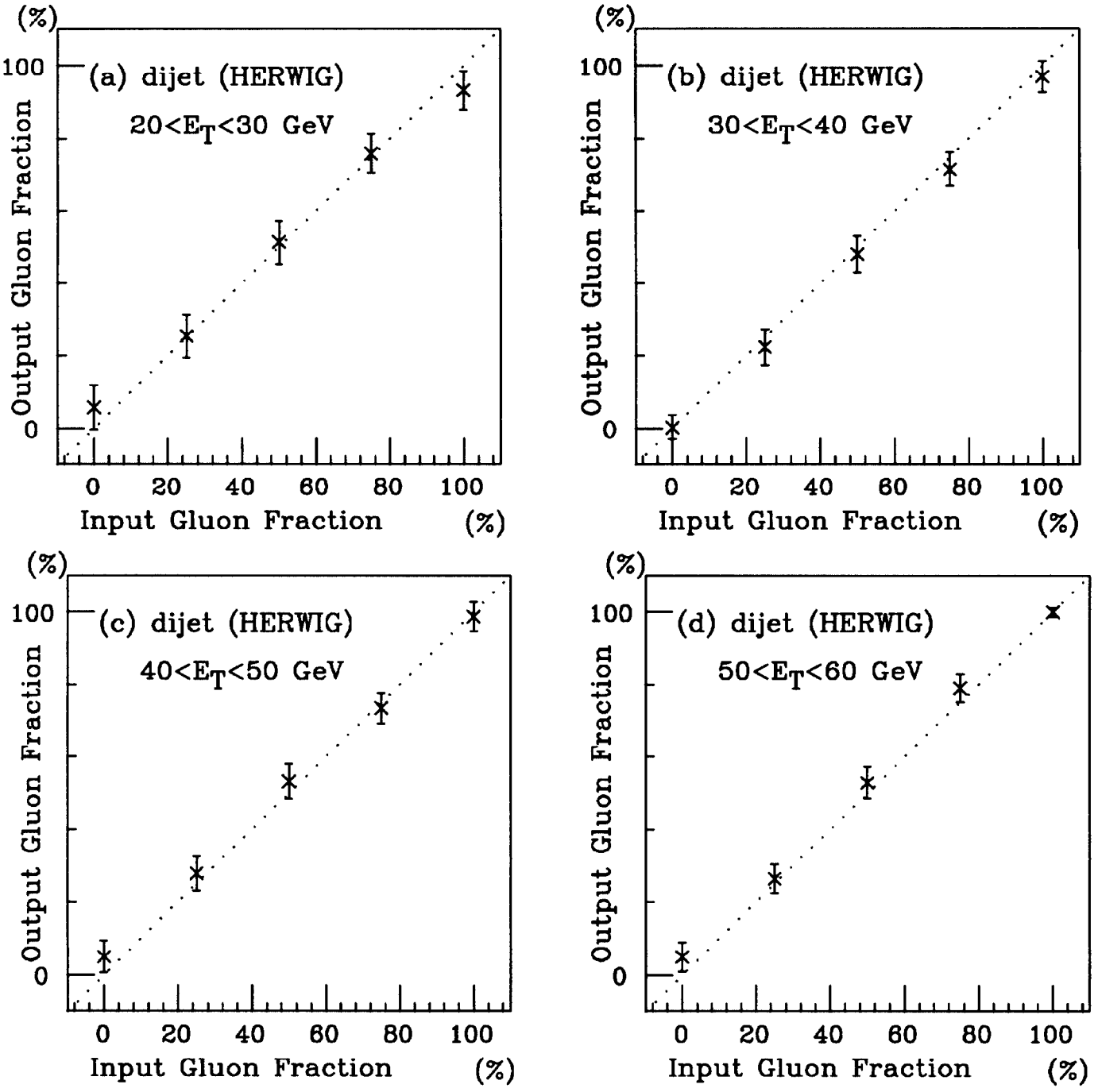

Figure 11: A Monte Carlo study of predictability of the gluon fraction found by the moment/likelihood analysis using mixed gluon and quark jet samples of known ratio. The referenced and analyzed jets were generated by the HERWIG Monte Carlo for dijet events: (a) in $20 < E_T < 30$, (b) in $30 < E_T < 40$, (c) in $40 < E_T < 50$ and (d) in $50 < E_T < 60$. 5000 jets per point were used in the reference jet sample and 1000 jets in the analyzed jet sample. The X coordinate shows the input gluon fraction and the Y coordinate the gluon fraction obtained in the analysis. The errors are obtained from a condition $\chi^2 = \chi^2_{min} + 1$.

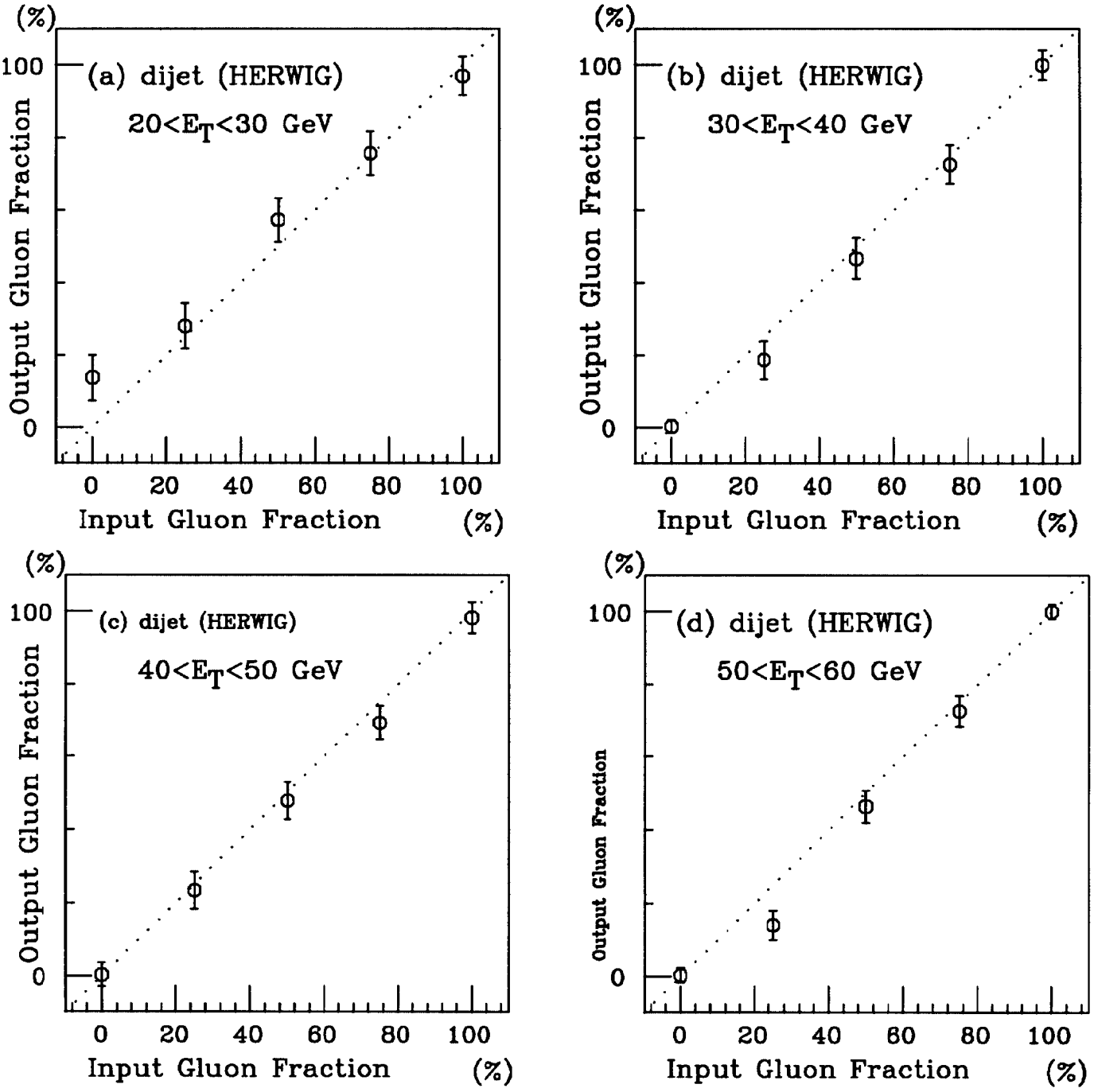

Figure 12: A Monte Carlo study of the analysis predictability as described in Figure 11, for the case of using the charged multiplicity distribution alone in the fit.

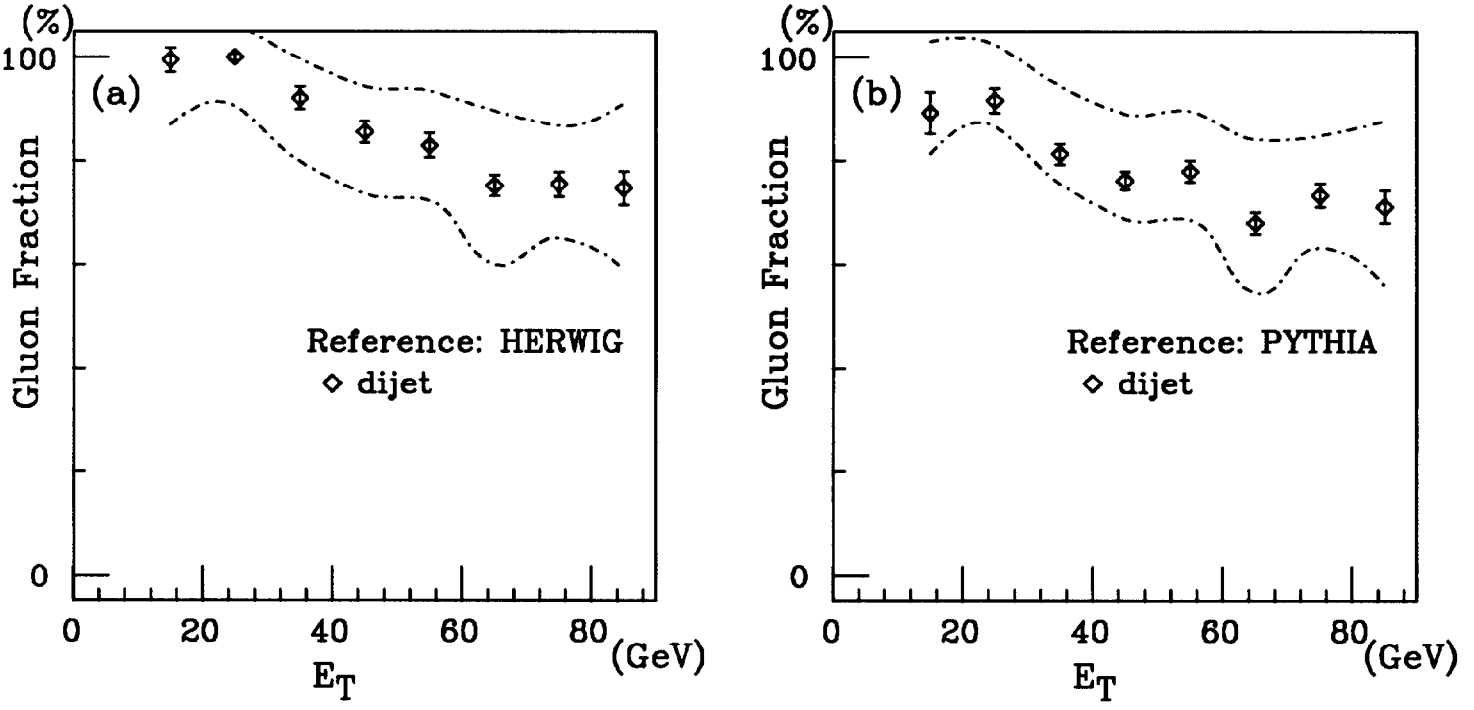

Figure 13: The gluon fraction in the dijet event sample obtained by the moments/likelihood method. The points are plotted at the mean value of E_T in each bin. The calculation of the fraction has been carried out using Monte Carlo event samples as reference quark and gluon jets, which were generated with (a) HERWIG and (b) PYTHIA, and simulated with a CDF detector simulator. The error bars show the statistical uncertainty obtained from a condition $\chi^2 = \chi^2_{min} + 1$ and the dot-dashed lines shows the total uncertainty obtained from a quadratic sum of the systematic and statistical uncertainties.

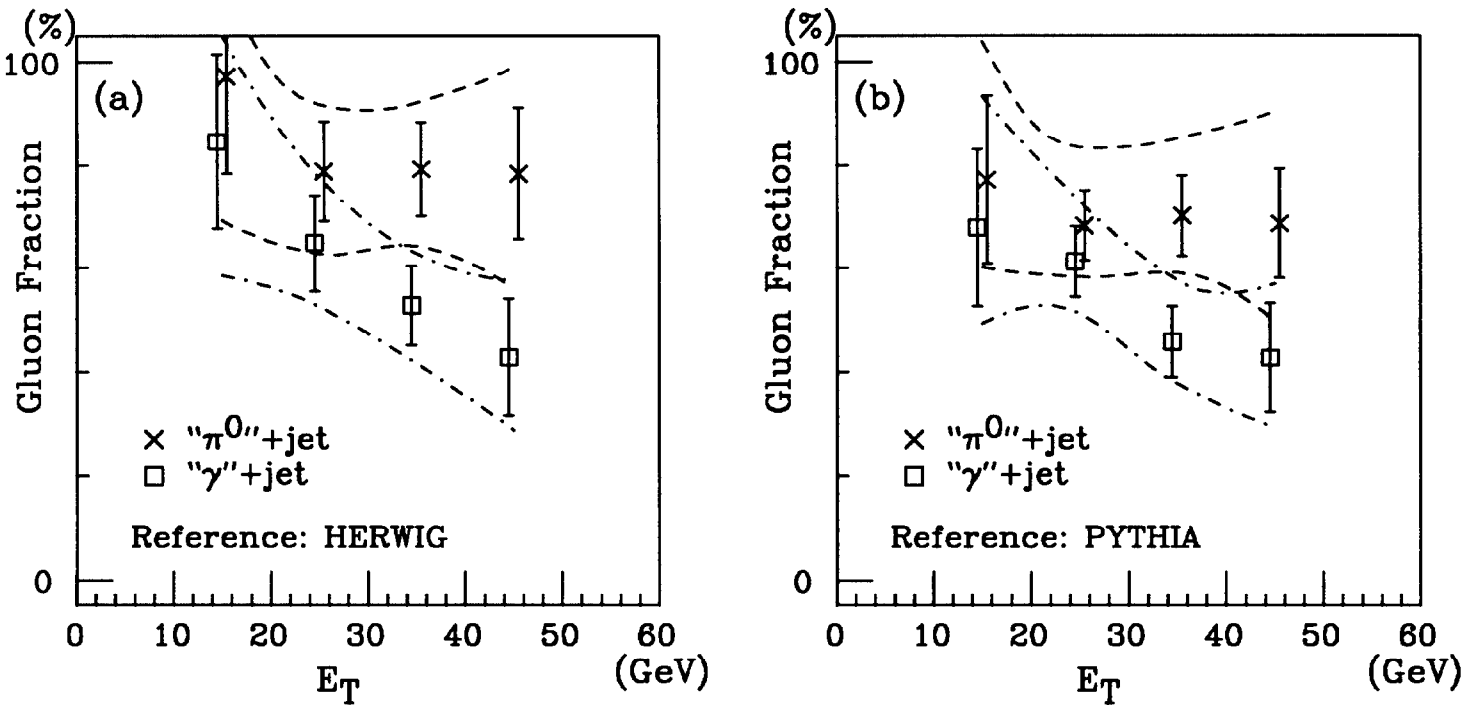

Figure 14: The gluon fraction in the "γ"+jet and "π^0"+jet event samples obtained by the moments/likelihood method. The plotted mean values of E_T are shifted by +1 GeV in the π^0+jet events and by −1 GeV for in the γ/π^0+jet events to distinguish them for reader's convenience. The error bars show the statistical uncertainty obtained from a condition $\chi^2 = \chi^2_{min} + 1$ and the dashed and dot-dashed lines show the total uncertainty in the "π^0"+jet and "γ"+jet samples, respectively.

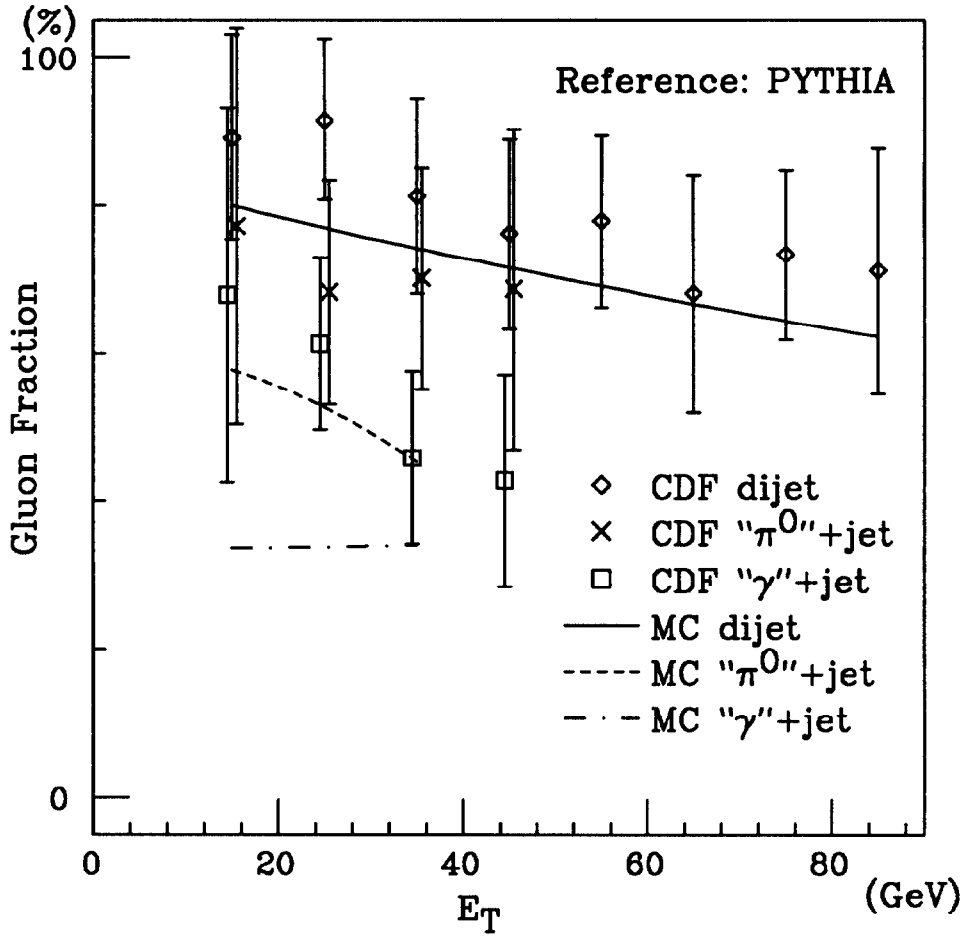

Figure 15: A summary plot of the gluon fraction in the dijet, "π^0"+jet and "γ"+jet event samples by the event generator PYTHIA. The points are obtained for the CDF data by the moments/likelihood method, and the errors are the total uncertainty obtained from a quadratic sum of the systematic and statistical uncertainties. The solid, dashed and dashed-dot lines show the Monte Carlo predictions for dijets with structure functions by MRS D'_, "π^0"+jet and "γ"+jet events, respectively.

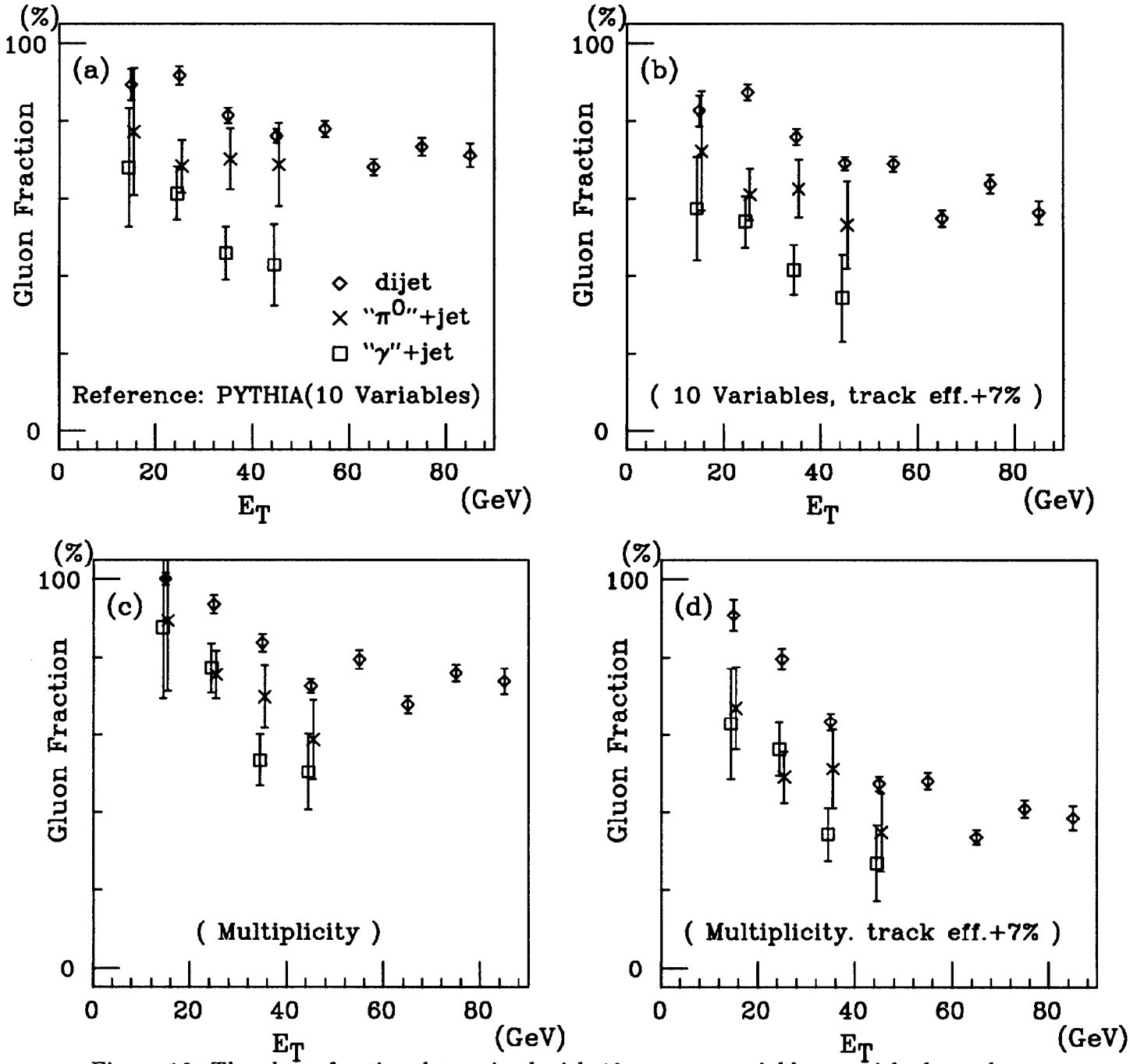

Figure 16: The gluon fraction determined with 10 moment variables or with charged multiplicity in the dijet, "γ"+jet and "π^0"+jet event samples. The track finding efficiency is set to $\sim$ 85 % in (a) and (c) and set to be higher by 7 % in (b) and (d), respectively, for the Monte Carlo simulation of the reference samples. The points are plotted at the mean value of E_T in each bin. The errors are obtained from a condition $\chi^2 = \chi^2_{min} + 1$.

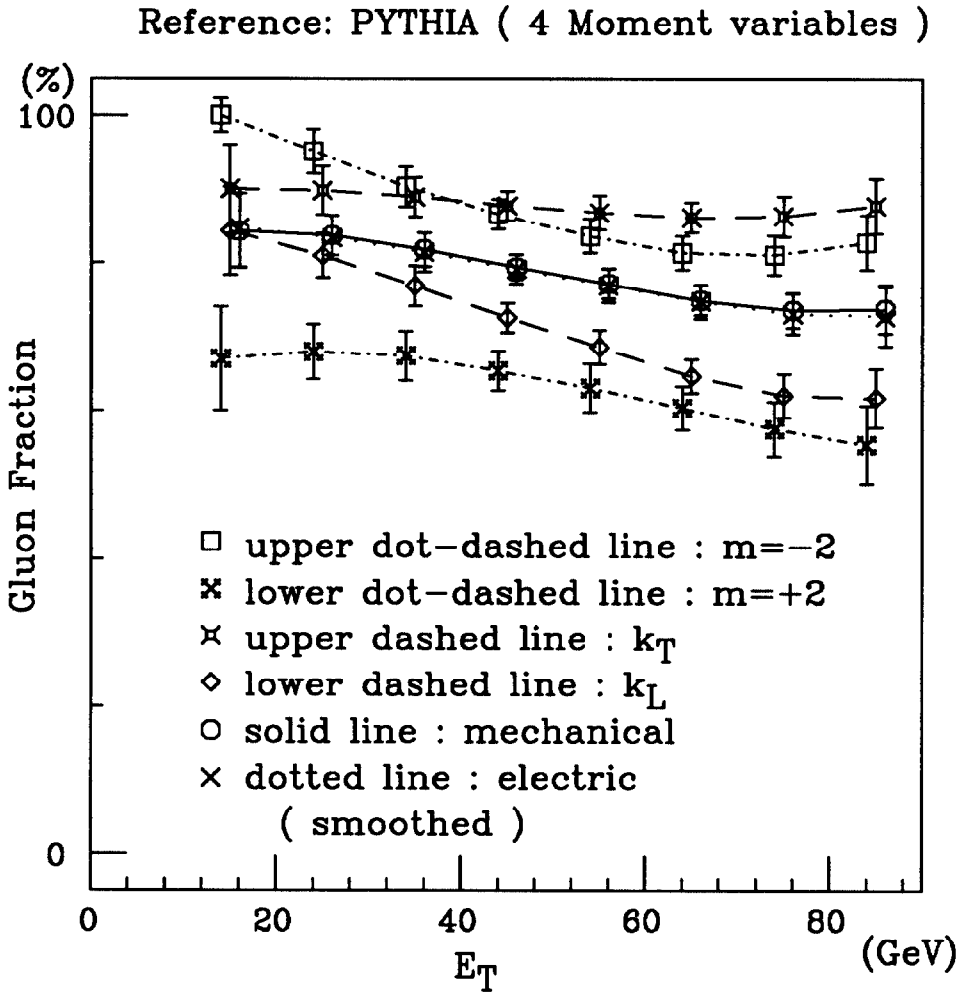

Figure 17: The gluon fraction in the CDF dijet data determined with different combinations of four moment variables in Table 3. The points are plotted at the mean value of E_T in each bin. The errors are obtained from a condition $\chi^2 = \chi^2_{min} + 1$.